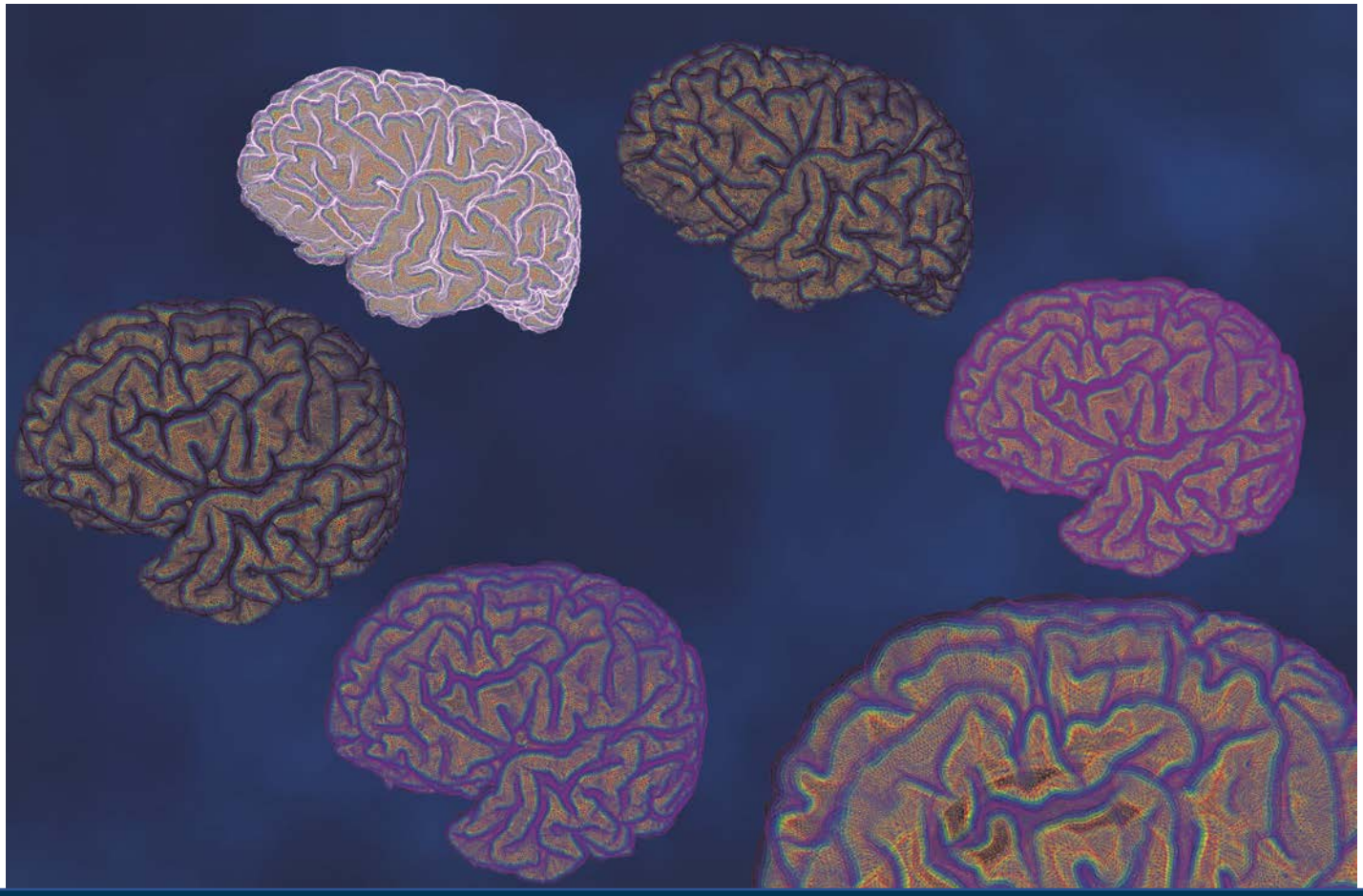

INM-4 ENHANCED DYNAMIC MR STUDIES USING EPI WITH KEYHOLE (EPIK)

Institute of Neuroscience and Medicine – 4
Medical Imaging Physics, Forschungszentrum Jülich GmbH, Germany

Mitglied der Helmholtz-Gemeinschaft

JÜLICH
Forschungszentrum

EPI WITH KEYHOLE (EPIK)

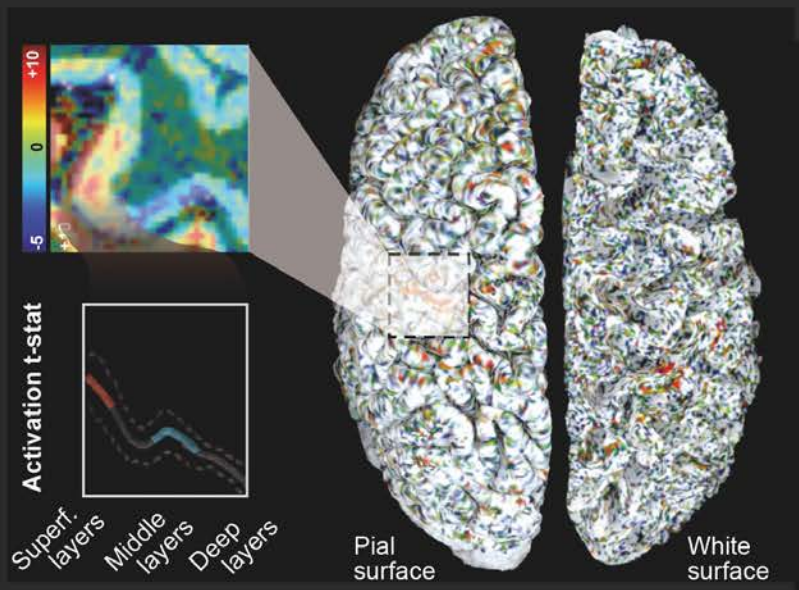

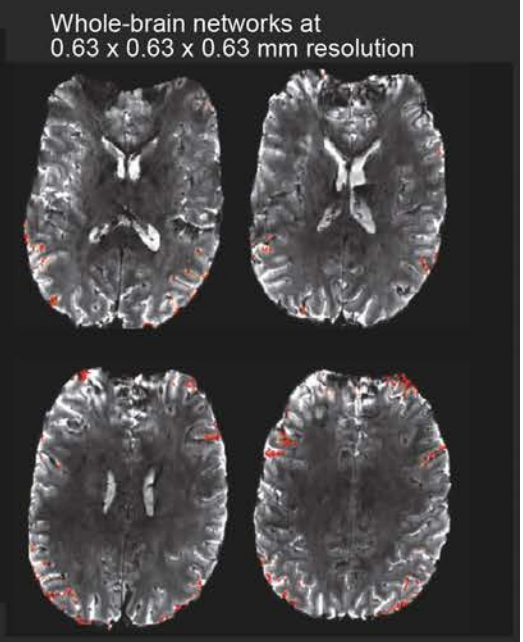

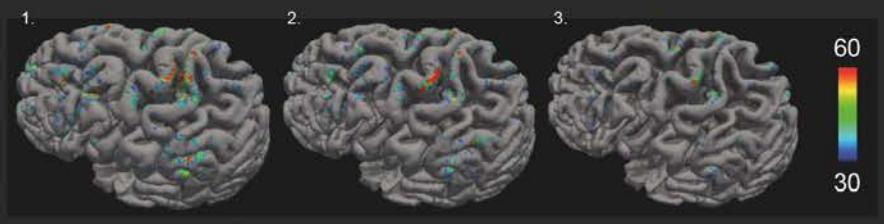

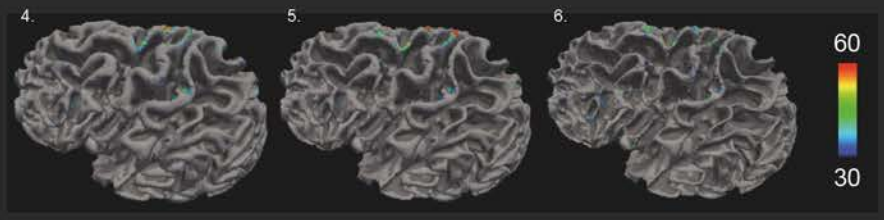

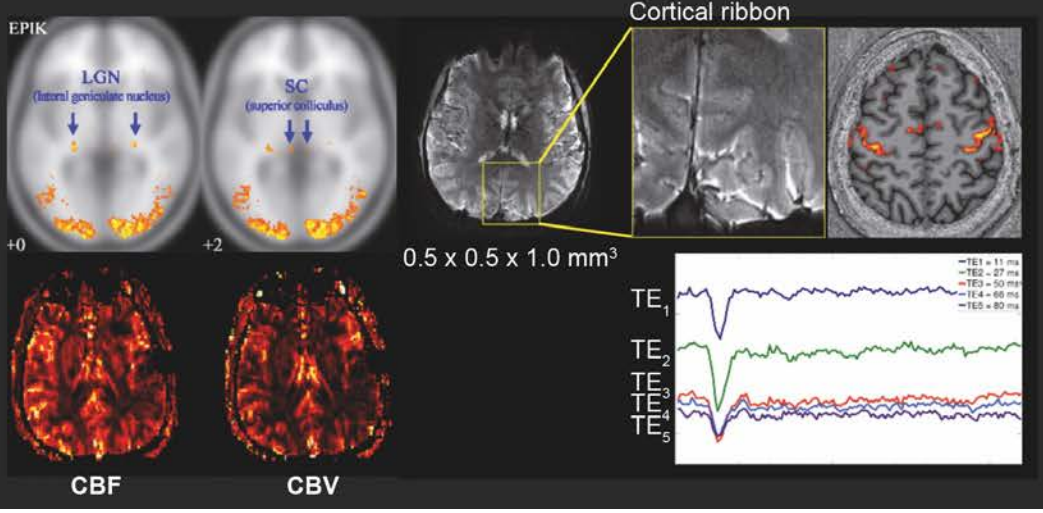

COVER ILLUSTRATION

(HBM)

Seong Dae Yun, Patricia Pais-Roldán, Nicola Palomero-Gallagher, N. Jon Shah

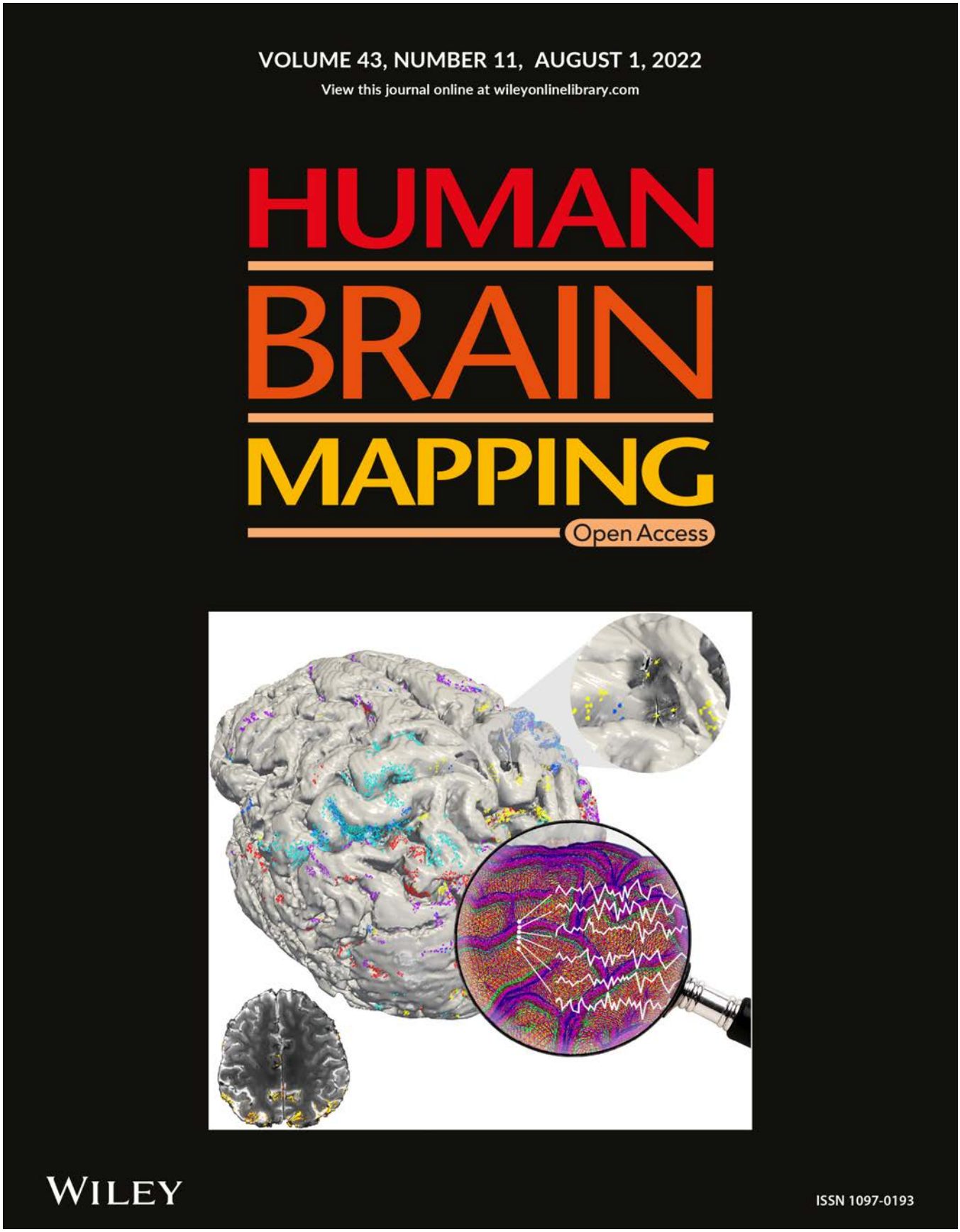

Mapping of whole-cerebrum resting-state networks with the half-millimetre in-plane voxel enabling the identification of cortical depth-dependent activation.

EPI WITH KEYHOLE (EPIK)

Acquisition strategy

EPIK is a hybrid imaging technique which overcomes many of the performance disadvantages associated with EPI. EPIK has been developed [1, 2] and validated at 1.5T, 3T and 7T with various applications, such as fMRI, perfusion and quantitative mapping of relaxation parameters [3-41].

As shown in the figure to the right, the EPIK acquisition consists of Nyquist sampling (Δky = 1/FOV) for central k-space **(keyhole)** and sparse sampling (Δky‘ = 3/FOV) for peripheral k-space – in which the black solid, dashed and fine-dashed lines are sampled during the 1st, 2nd and 3rd scans, respectively, like three-shot EPI.
Here, the missing k-space lines in the peripheral k-space are reconstructed with a sliding-window reconstruction.

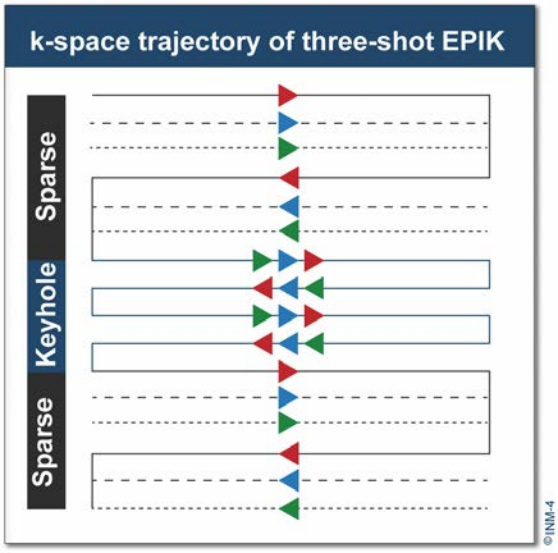

Higher temporal resolution

In general, higher-resolution MRI requires increased scanning time, which may be a critical constraint to derive a particular contrast or for scanning patients with motion control abnormalities. In EPIK, the number of phase-encoding lines required to encode a single-slice of k-space data can be effectively reduced, which enables **dynamic MRI with a shorter acquisition time.** In our early works, several EPIK configurations have been demonstrated [5,6,12] and a substantial reduction in scanning time has been achieved (see the table below).

Matrix size	Resolution (mm^2)	# keyhole lines	iPAT	Acceleration rate
96 x 96 [5]	2.5 x 2.5	24	2	4.0
240 x 240 [6]	1.0 x 1.0	60	2	4.8
408 x 408 [12]	0.5 x 0.5	48	3	10.5

Configuration of EPIK parameters

Robustness against distortions

The figure below shows reconstructed in vivo slices acquired with EPI (community standard fMRI protocol) and EPIK at identical slice positions [5]. The EPIK scan is observed to have **substantially reduced geometric distortions** compared to the EPI scan (see the regions marked by arrows). To aid comparison, a GRE image is displayed alongside as a reference.

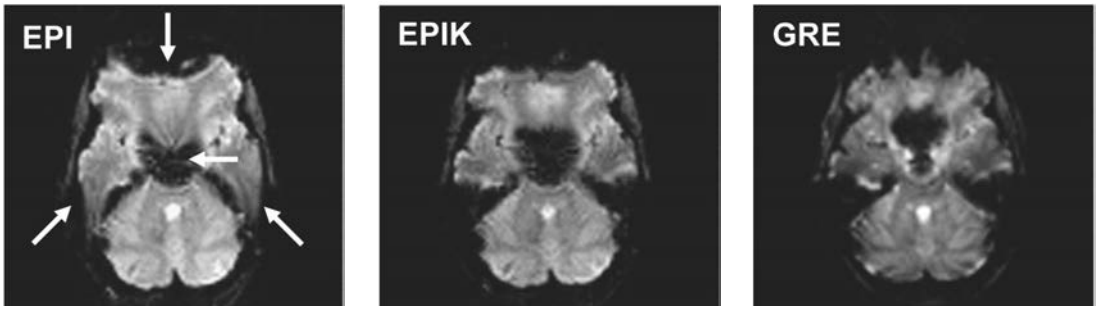

EVALUATION OF EPIK
SIMULATIONS

Point spread function (PSF)

The degree of image blurring in an EPI-based method can be measured by simulating its signal decay trajectory as a function of the sampled k-space line. The figure below (left) depicts the signal decay tra-jectories of EPI, three-shot EPI and EPIK. The signal decay plot of EPIK is not smooth due to the different sampling rates for central and peripheral k-space. However, the continuous and monotonic decrease of the signal can prevent the occurrence of major image artefacts such as ghosts. The PSF of EPIK (right figure) has a narrower shape than the EPI case, indicating that EPIK results in **fewer image blurring artefacts (i.e. better spatial resolution) [5].**

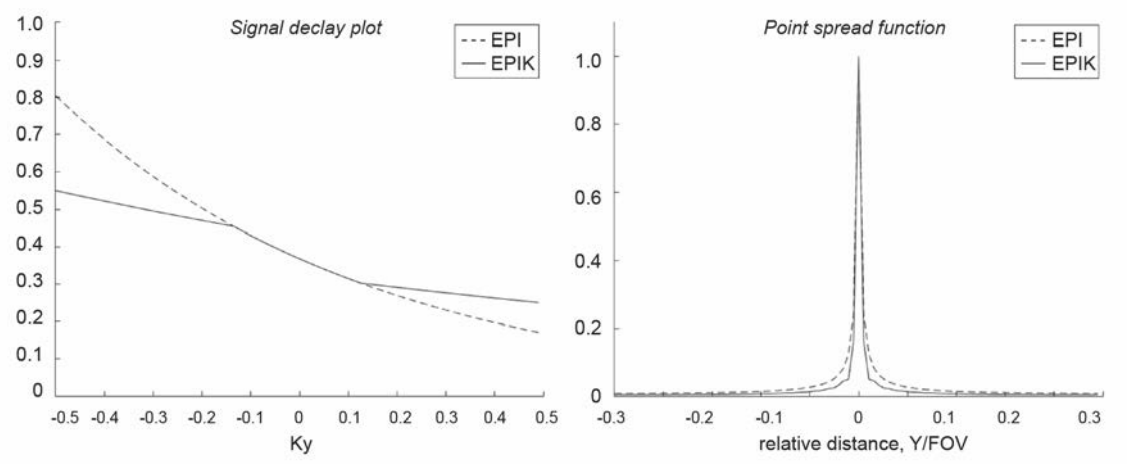

BOLD simulation

The performance of each imaging method for the detection of BOLD signals has been investigated using an fMRI data set generated by an MRI simulator - JEMRIS (Jülich Extensible MRI Simulator). The sequences em-ployed in this simulation are two-fold accelerated EPIK and four-fold acce-lerated EPI; both sequences have an identical reduction factor [5].

Five small, square-shaped activation regions (marked by yellow squares in the figure right) were defined inside the simulation phantom. The artificial BOLD signal was designed so that the peak signal change was 5% of the baseline (see the fine-dashed line in the bottom right figure). As depicted in the figure, the BOLD response from the accelerated EPIK method shows excellent agreement with the originally designed one, which is not the case with accelerated EPI. This simulation result suggests that EPIK can be effectively deployed in fMRI.

Simulation phantom with activation spots

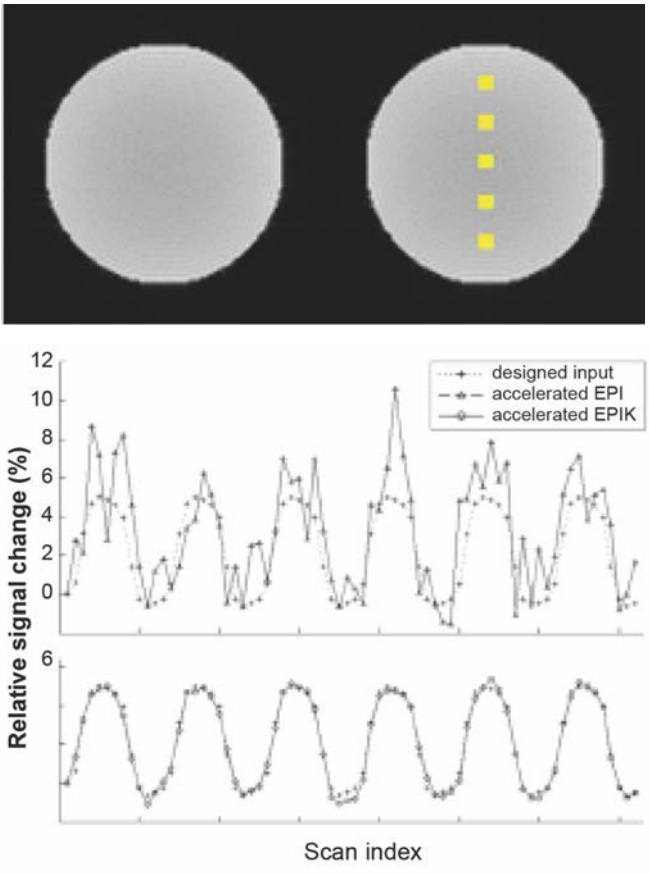

EVALUATION OF EPIK
fMRI AT 3T

Design of fMRI & data recon

In order to demonstrate the feasibility of EPIK for fMRI, three different reconstructions (single-shot EPI, three-shot EPI and EPIK) were performed for the same fMRI data set. The fMRI data set was obtained using single-shot EPI, which is considered as a reference against the other two different reconstructions (three-shot EPI and EPIK). Sixteen healthy volunteers (8 males; mean age, 28.44 years; range, 22-38) were recruited and a visual checkerboard paradigm was employed to elicit circumscribed activation in the visual cortex [6].

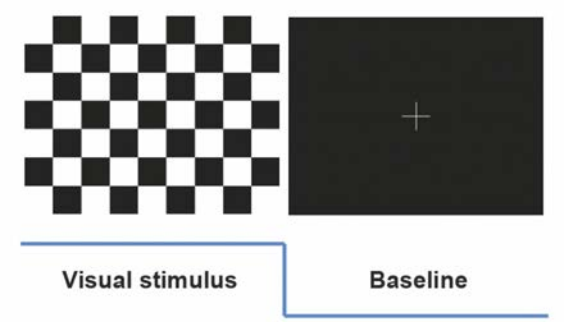

Visual checkboard paradigm

	Parameters
TR/TE	3000/35 ms
FOV	240 x 240 mm^2
Matrix	96 x 96 (2.5 x 2.5 mm^2)
# of slices	25 (10% gap)

Employed imaging parameters

fMRI activation

The figure below presents one-sample t-test results (an uncorrected p-value < 0.001) for the three recon-structed data sets. Visual inspection of the figure suggests that **the results from EPIK have features very comparable to those of EPI,** whereas the activation area from multi-shot EPI are substantially reduced when compared to EPI. The table below shows the statistical quantities examined for several functional ROIs: V1 ~ V5 and lateral geniculate nucleus (LGN). The values in the table are presented in the following order: EPI/three-shot EPI/EPIK. **The results reveal that the**

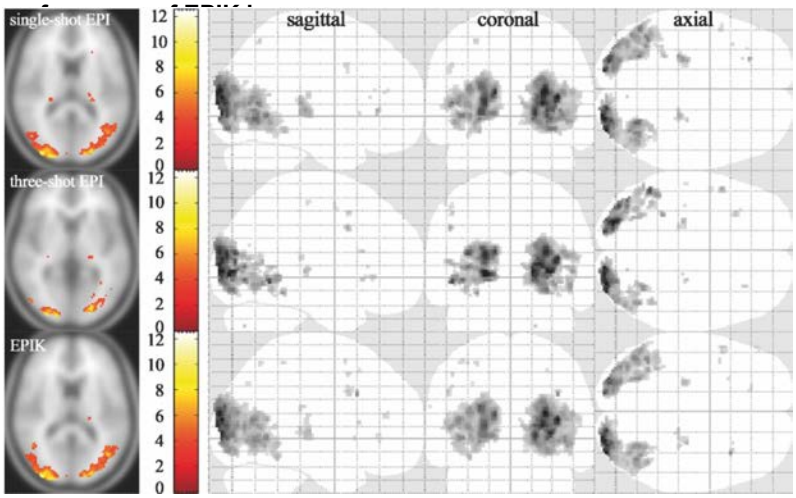

parable to that of EPI in terms of all examined statistical quantities. However, in three-shot EPI, considerable perfor-mance degradation was observed in the number of detected voxels. For EPIK, 85.3 % of the iden-tified voxels have exactly the same functional lo-cations as EPI, where-as only 47.2 % exactly match for three-shot EPI.

ROI	Maximum t-value	Mean t-value	# detected voxels	MNI coordinates (X, Y, Z)
V1	9.50/9.37/10.03	4.91/5.25/5.06	182/120/165	18 -92 0/16 -94 2/18 -92 0
V2	7.19/6.49/7.05	4.77/4.81/4.78	40/32/42	22 -96 18/22 -96 18/22 -96 18
V3	11.15/10.04/11.79	5.91/5.55/5.98	555/486/576	26 -94 18/30 -92 2/26 -94 18
V4	6.98/6.42/5.96	4.54/4.40/4.36	58/34/66	32 -86 -12/-22 -84 -4/-20 -82 -2
V5	5.51/6.74/5.16	4.26/4.29/4.29	58/27/50	44 -70 0/ -40 -74 -4/44 -66 0
V6	6.12/5.03/5.33	4.36/4.18/4.20	154/16/80	-24 -26 2/-22 -26 2/-22 -24 2

FINGER-TAPPING
FMRI EPI AT 3T

fMRI design

The putative enhanced sensitivity of EPIK has been examined using 'visually guided finger tapping' fMRI to demonstrate the advantages of EPIK for fMRI at 3T. The acquired data were directly compared to the community standard fMRI protocol using single-shot EPI to ascertain a clear comparison. The effect of each sequence on effective connectivity has also been inspected using dynamic causal modelling (DCM) [10].

fMRI protocols

Each EPI and EPIK sequence was optimised to offer its highest possible spatial resolution under the condition that the other imaging parameters were kept identical: FOV = 200 × 200 mm², flip angle = 90°, TR/ TE = 2200/30 ms and slice thickness = 3 mm with a distance factor of 10%. In this way, **higher spatial resolution and increased slice coverage was achieved with EPIK** (see table – right).

	EPI	EPIK
Matrix size	64 x 64	96 x 96
Res. (mm²)	3.13 x 3.13	2.08 x 2.08
# of slices	36	32

Higher sensitivity

Both EPI and EPIK consistently revealed significant activations for motor and visual brain regions (see Fig. a below). However, **EPIK revealed stronger BOLD amplitudes for several brain regions** (see Fig. b and the table below). Moreover, effective connectivity analyses using a DCM model (see figure – below right) indicate that EPIK and EPI have a similar performance for task-induced connectivity changes between brain regions. However, the coupling parameters of the intrinsic connection between the hand area and the right visual area had a **significantly smaller variance (i.e. reliable estimation) in EPIK** compared to EPI.

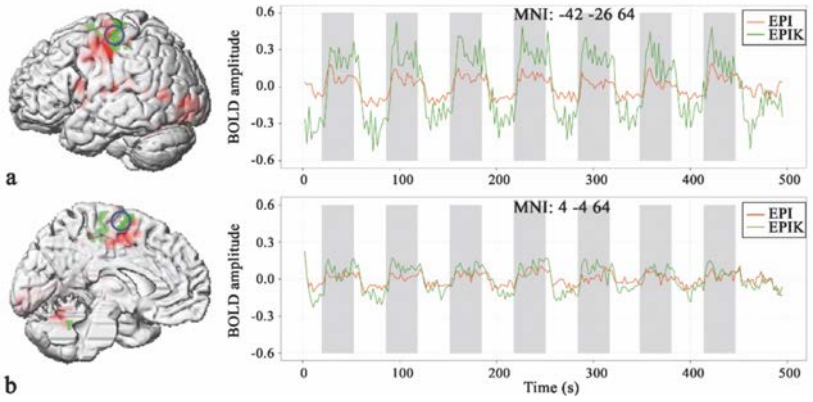

Time course at the maximally activated voxel from: (a) M1 and (b) SMA

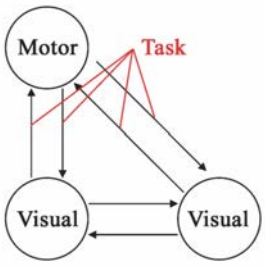

DCM model for effective connectivity analysis

Brain region	Cluster size	Side	MNI-coordinates	T-Score
Pre-/Postcentral gyrus	132	L	-42 -26 64	7.56
Medial frontal cortex/SMA	82	R	4 -4 64	6.66
Inferior/Middle occipital gyrus	39	R	36 -78 -2	7.04
Cerebellum	32	R	20 -48 -28	6.37
Cerebellum	29	R	6 -58 -24	6.94

Brain regions showing higher activity by EPIK.

Brain region	Hand	Visual left	Visual right
Hand	F (13,13)= 0.68787 p=1 n.s.	F (13,13)= 0.49456 p=1 n.s.	F (13,13)= 1.4384 p=1 n.s.
Visual left	F (13,13)= 0.54103 p=1 n.s.	F (13,13)= 0.45834 p=1 n.s.	F (13,13)= 1.11 p=1 n.s.
Visual right	F (13,13)= 4.8796 p=0.033	F (13,13)= 0.71235 p=1 n.s.	F (13,13)= 0.91628 p=1 n.s.

F-scores and p-Values testing for lower variance in EPIK.

ACCELERAT ED EPIK
HIGH-RESOLUTION IMAGING

High-resolution imaging

The EPIK scheme can be further accelerated with parallel imaging and partial Fourier techniques to achieve even higher resolution in fMRI; the figure (right) shows schematic representations of the two acceleration techniques where the dotted lines indicate skipped lines. The high resolution afforded by EPIK can be exploited in applications investigating relatively small functional areas.

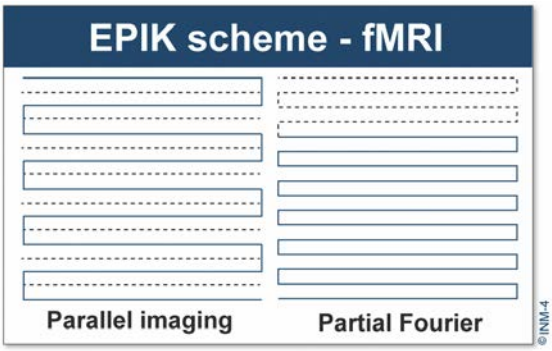

High-resolution imaging

For the figures shown below, the imaging parameters for EPIK were optimised in such a way so that the maximum achievable matrix size and number of slices were provided under the given imaging conditions: FOV = 240 × 240 mm^2, flip angle = 90°, TR/TE = 3000/35 ms and slice thickness = 4 mm (10% gap). The EPI sequence was also optimised in the same way (see table below).

Method	Matrix size	Resolution	# of Slices	Acceleration
EPI	192 x 192	1.25 x 1.25 mm^2	28	Parallel imaging (2) + Partial Fourier (6/8)
EPIK	240x 240	1.00 x 1.00 mm^2	32	

©INM-4

Anatomical structures in high-resolution

From the left figure below, it can be seen that the higher spatial resolution of EPIK (1.00 × 1.00 mm^2) enabled clearer identification of the boundaries between grey and white matter compared to EPI (1.25 × 1.25 mm^2) (see the regions marked by black arrows). In an additional set of slices, shown on the right, significantly reduced geometric distortions were observed in the EPIK image, particularly around the marked white arrows; signal drop-out induced by the susceptibility differences around the frontal lobe is significantly less in EPIK than in EPI.

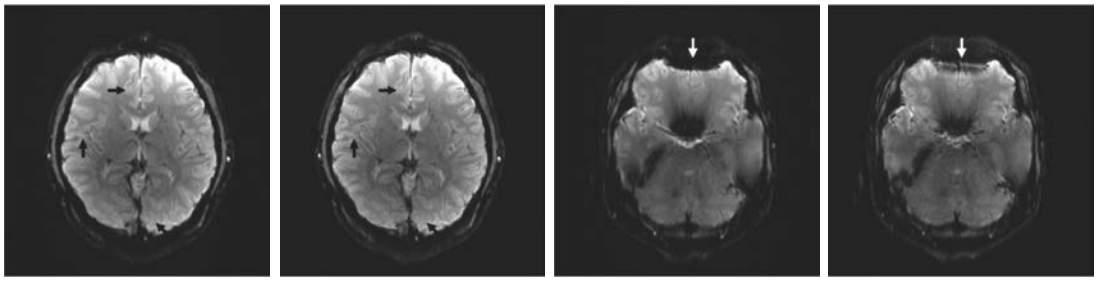

The above slices show that **higher resolution imaging of EPIK enables a clearer identification** of the boundaries between grey and white matter than EPI (see the black arrows).

The above slices show **better performance of EPIK in terms of robustness against susceptibility difference,** when compared to EPI (i.e. less signal drop-out around the frontal lobe).

HIGH-RESOLUTION fMRI
EPIK AT 3T

fMRI design

A visual checkerboard paradigm was employed for in vivo fMRI experiments to elicit circumscribed activation in the visual cortex. The imaging protocol consisted of six dummy scans for reaching a steady state, and 72 scans comprising six cycles of baseline-activation states, each lasting six volume acquisitions for a total of 18 seconds. Sixteen healthy volunteers (10 males, 6 females; mean age, 28.88 years; range, 20-42 years) participated in the study [6].

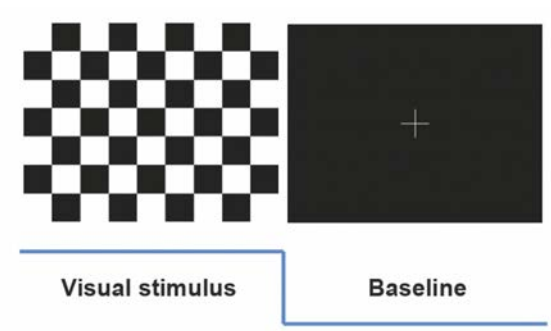

Visual checkboard paradigm

	EPI	EPIK
Matrix size	192 x 192	240 x 240
Res. (mm²)	1.25 x 1.25	1.00 x 1.00
# of slices	28	32

Imaging parameters of EPI and EPIK

Method evaluation

The performance of high-resolution EPIK was directly compared to that of high-resolution EPI (community standard) and its potential advantages were investigated with visual fMRI experiments. The imaging protocols provided by each method are shown in the table above.

Detection of small functional region: LGN & SC

The bottom middle figure shows activation patterns obtained from one representative subject. It was observed that activations were largely identified around the visual cortex in both imaging methods, but **the activations from EPIK were distributed more precisely along with the cortical area** compared to those from EPI. The bottom right figure shows activation patterns obtained from a 16-subject group. Besides the visual cortex, LGN and SC (see bottom left figure) were also recognised as activation regions, although illustrating rather smaller activation volumes. From this figure, it can be observed that **the LGN and SC regions were better characterised by EPIK than EPI.**

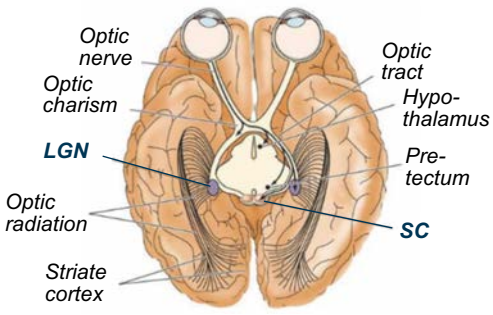

LGN (Lateral Geniculate Nucleus): transit of visual information
SC (Superior Colliculus): control of eye movements

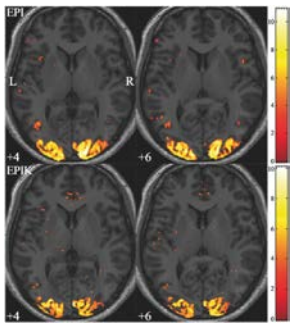

Result from a representative subject

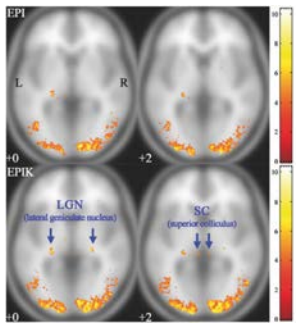

Result from a 16-subject group

DUAL-CONTRAST EPIK
PERFUSION IMAGING

Dual-Contrast EPIK

The EPIK scheme can be configured to provide dual contrasts (DC-EPIK) for dynamic susceptibility contrast MRI. As shown in the acquisition diagram (right): The "time" axis is present for the different contrasts (TE_1 and TE_2) and the "repetition" axis is present for the temporal scans (A, B, and C) where data sharing of peripheral k-space lines takes place. For the given conditions (see the table right), EPIK yielded dual contrasts (13 ms and 33 ms) with 24 slices, whereas EPI only provided single contrast (32 ms) with a decreased slice coverage (20 slices) [7,8].

	EPI	EPIK
FOV	230 x 230	
Matrix size (Res.)	128 x 128 (1.80 x 1.80 mm^2)	
# of slices	20	24
TEs	32 ms	13/33 ms

©INM-4

Imaging parameters of EPI and EPIK

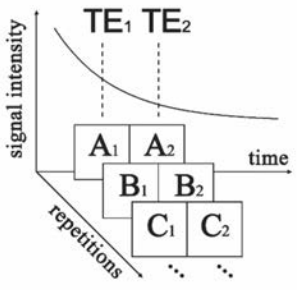

Acquisition diagram of DC-EPIK

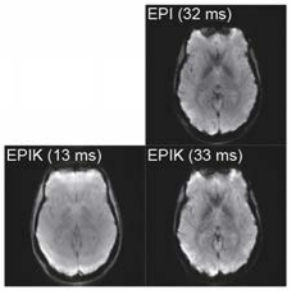

Acquisition diagram of DC-EPIK

AIF an CBF/CBV

The figure on the right depicts the estimated arterial input function (AIF), obtained from EPI, EPIK (TE_1), EPIK (TE_2) and EPIK using both echoes. The curve peak from EPIK (TE_1) is higher than in other cases due to the use of a shorter TE. The peaks from the other three curves have similar amplitudes and temporal location, which demonstrates the performance of EPIK in AIF estimation. In the figure below, the images in the first and second columns were acquired before and after the contrast injection. The effect of the contrast agent on the image contrast can be clearly seen in both EPI and EPIK. The arrows indicate the area where contrast leakage occurred due to the presence of a tumour. The effect of contrast leakage can be effectively corrected using the dual contrasts in EPIK, resulting in **better parametric images (CBF & CBV)** (see the third and last columns below).

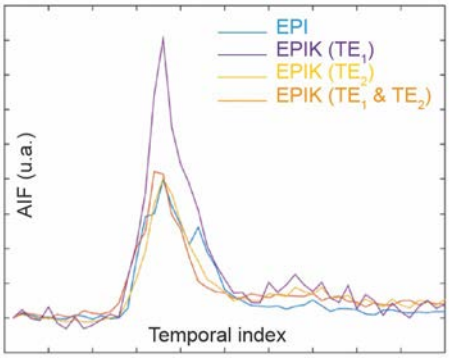

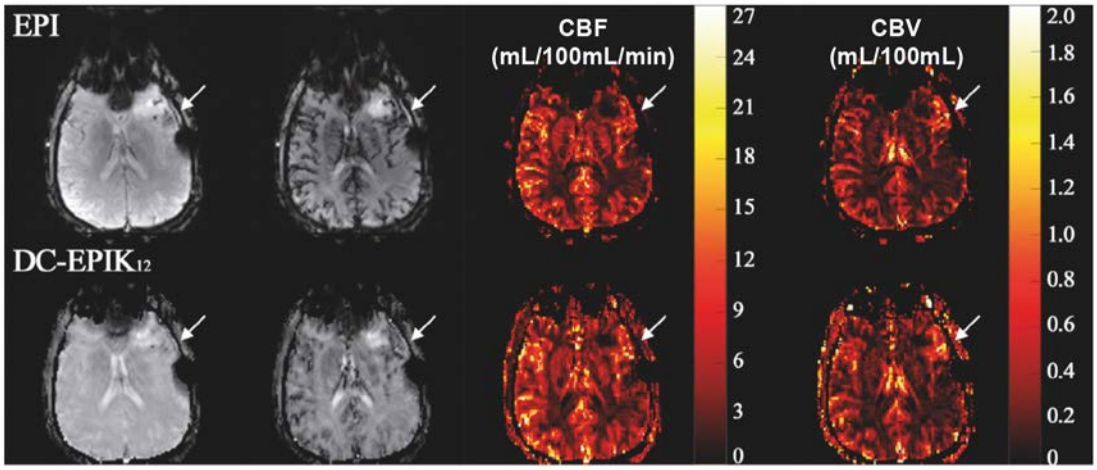

FIVE-ECHO GESE EPIK
PERFUSION IMAGING

Five-echo GESE EPIK

A more thorough and versatile investigation of tumours, including information about the vasculature, can be carried out by combining gradient-echo (GE) and spin-echo (SE) signals. For this purpose, the original GE-EPIK has been extended to a GESE version to provide five echoes: two with GEs, two with mixed GESE and one with SE (see the figure below) [7,9].

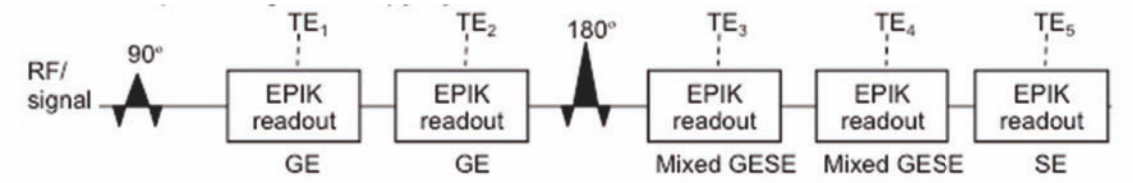

Schematic sequence representation for GESE-EPIK with five echoes

Contrast tracking / Parametric images

The figure above shows reconstructed images for all of the five echoes from GESE EPIK at baseline and at peak contrast passage. The figure (bottom right) illustrates the time course plot of the signal intensity, depicting the arrival of the contrast agent at a single, representative grey matter voxel. For all echoes, it was possible to clearly track the dynamic signal changes induced by the contrast agent even though a higher signal drop was found in earlier echoes when compared to the later echoes. The middle figure (right) presents tumour delineation obtained from PET data and GESE-EPIK parametric images. The values of CBF and CBV are higher in the GE data than those in the SE data. The hottest voxels from the FET-PET image are not in agreement with the maximum value of the perfusion-weighted images in either GE or SE, suggesting that the EPIK GE and SE contrasts present additional information. In addition, vessel size images are also obtained where different vessel organisation in the tumour can be observed when compared to contralateral areas.

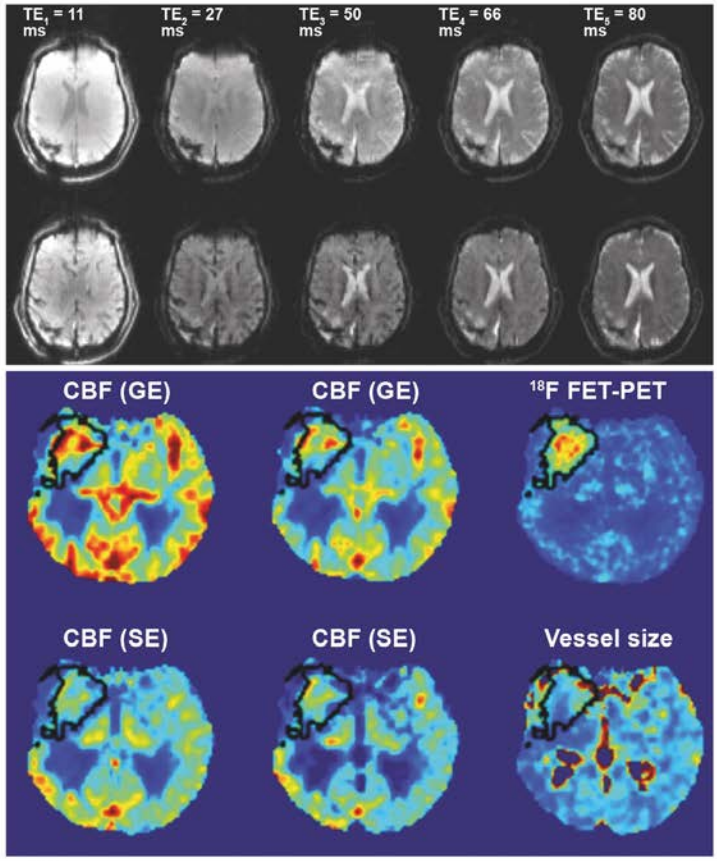

TEN-ECHO GESE EPIK
QUANTIFICATION OF T_2 AND T_2^*

Ten-echo GESE EPIK

Relaxometry quantification relies on multi-contrast multi-echo data. However, multi-echo sequences based on an EPI readout often require relatively large TEs for later echoes, resulting in reduced SNR and reduced slice coverage for a given TR. This GESE method aims to provide 10 echoes (i.e. two with GEs, six with mixed GESE and two with SE), enabling fast and simultaneous quantification of T_2 and T_2^* relaxation times (see figure below) [Küppers 2022].

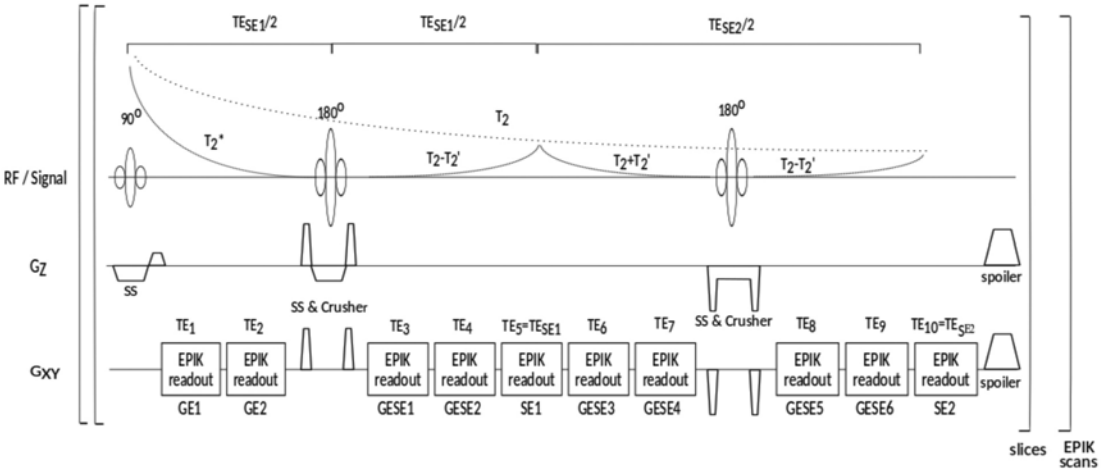

Schematic sequence representation for GESE-EPIK with ten echoes.

Images / T_2 and T_2^* maps

The figure below depicts reconstructed images, showing 10-echo images at a representative slice location revealing the contrast evolution over echo times. The second figure shows representative T_2 and T_2^* along with the main acquisition parameters. For validation purposes, the histogram comparison of the T_2 and T_2^* maps reveals a good agreement of T_2/T_2* values with those from established reference methods and also with the known values from the literature.

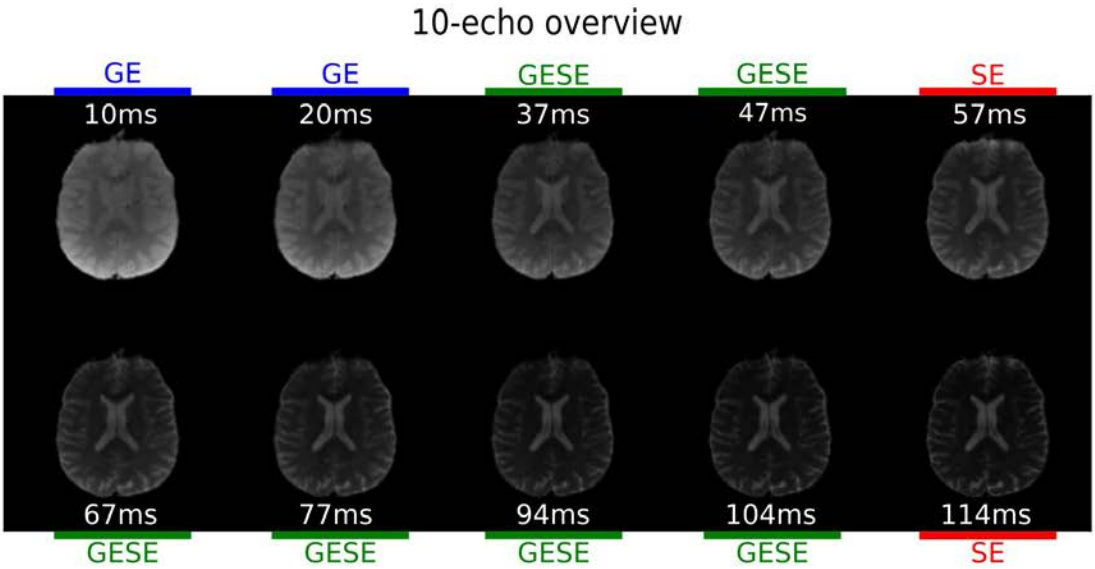

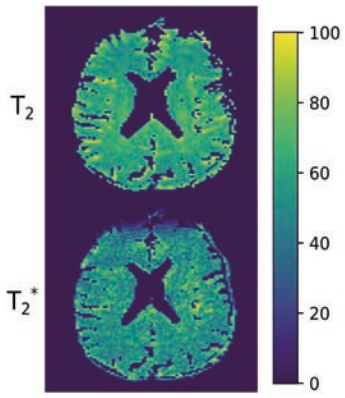

Relaxometry maps

TR/TE	2.8 s
FOV	240 x 240 mm²
Matrix (Res. mm²)	128 x 128 (1.88 x 1.88 mm²)
# slices	20 (3 mm thick.)
Acquisition time	0:57 min

Measurement Parameters

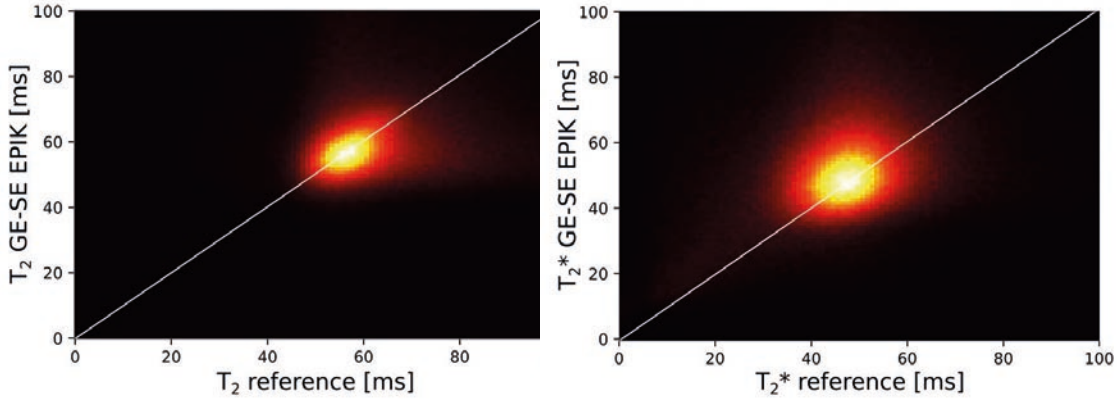

Quantification Validation with Reference Methods

Oxygen extraction fraction (OEF)

The oxygen extraction fraction (OEF) is a valuable biomarker to describe brain health and its metabolism. While the standard access is provided by PET measurements, logistic challenges as well as the radioactivity of the required tracer bring non-invasive MR methods into the focus. A recent approach makes advantage of the relationship between OEF and T_2', where latter one is characterised by the combination of T_2 and T_2*. Here, the proposed 10-echo GESE-EPIK sequence offers the potential to quantify OEF. A successful validation for healthy in vivo subjects revealed good agreement with expected literature values. During breath-holding experiments, a good sensitivity of the proposed method to challenge-related changes have been shown.

In the future, our research group aims to investigate the potential benefit and informative value of the MR derived OEF values in different clinical applications, such as hybrid MR-PET studies on brain tumour patients, as well as its correlation with existing clinical biomarkers [Küppers, 2023, ISMRM].

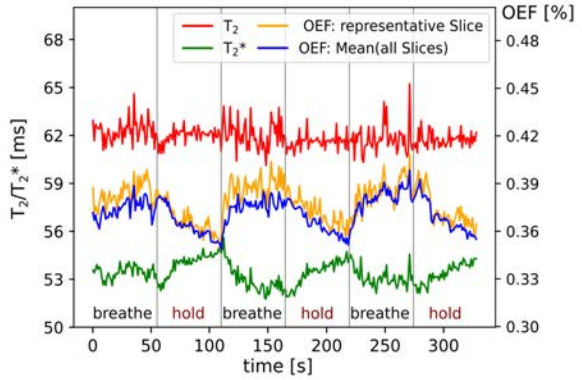

Time envelope for a single volunteer

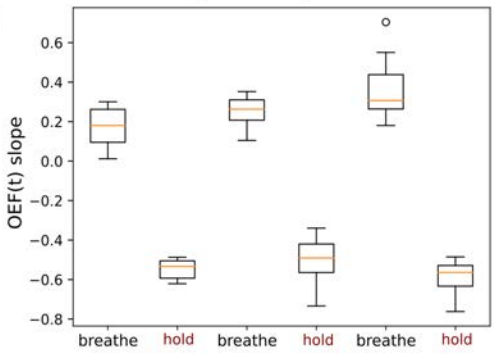

OEF slope of a single volunteer

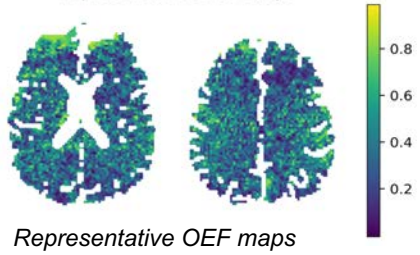

Representative OEF maps

INVERSION RECOVERY EPIK
T_1 MAPPING

Inversion recovery EPIK (ir-EPIK)

Due to their relative insensitivity to B_1 inhomogeneities, Look-Locker methods are widely used for the quantification of T_1 relaxation time. One such Look-Locker method, TAPIR, has been demonstrated with several clinical applications and has been shown to be faster than conventional gradient-echo sequences. However, it still requires considerable time for whole-brain imaging. The use of inversion recovery EPIK (ir-EPIK) aims to provide a much faster and whole-brain-covering Look-Locker method (see figure below) [27,29,30].

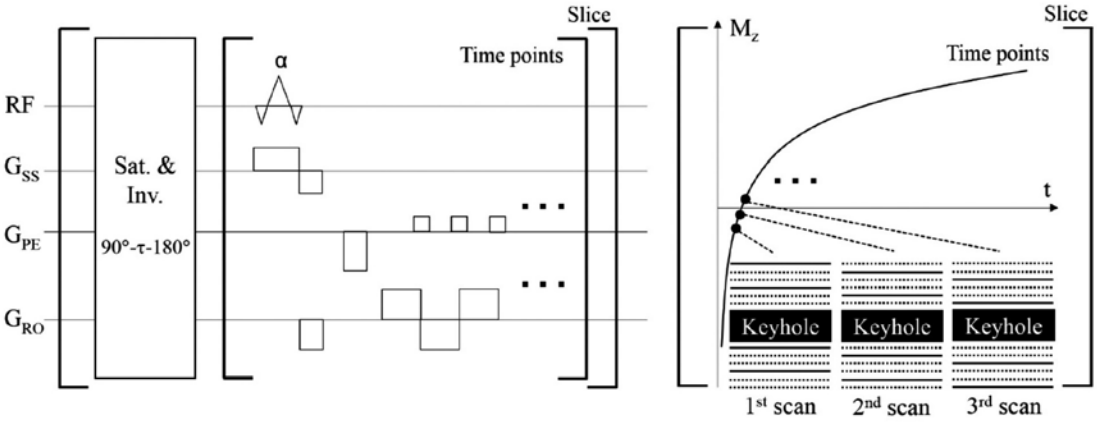

Sequence diagram of ir-EPIK

TAPIR vs. ir-EPIK In T_1 maps

Data sets from twenty subjects (10 males, 10 females; mean ± SD age, 28.20 ± 4.99 years) were acquired using both TAPIR and ir-EPIK at 3T. Two ROIs (i.e. WM and GM) from each imaging method were defined and the corresponding mean ± SD T_1 values were obtained. The estimated T1 values from ir-EPIK were comparable to those from TAPIR but were found to be slightly higher – around 6.84 % and 3.67 % higher for the WM and GM regions, respectively (see the table below. However, the estimated T_1 values are in good agreement with those from previous literature. In addition, EPIK enabled whole-brain T_1 mapping with the T_1 recovery data (2.5 mm^2 re-solution × 49 slices × 63 time-points) acquired within 5 minutes. The figure below shows the T_1 maps for all 49 slices from ir-EPIK, showing that reliable T_1 estimation was performed for all slices [27,29,30].

	WM (ms)	GM (ms)
TAPIR	934.16 ± 36.19	1538.84 ± 46.98
ir-EPIK	998.03 ± 26.40	1595.36 ± 44.18

Estimated T_1, values

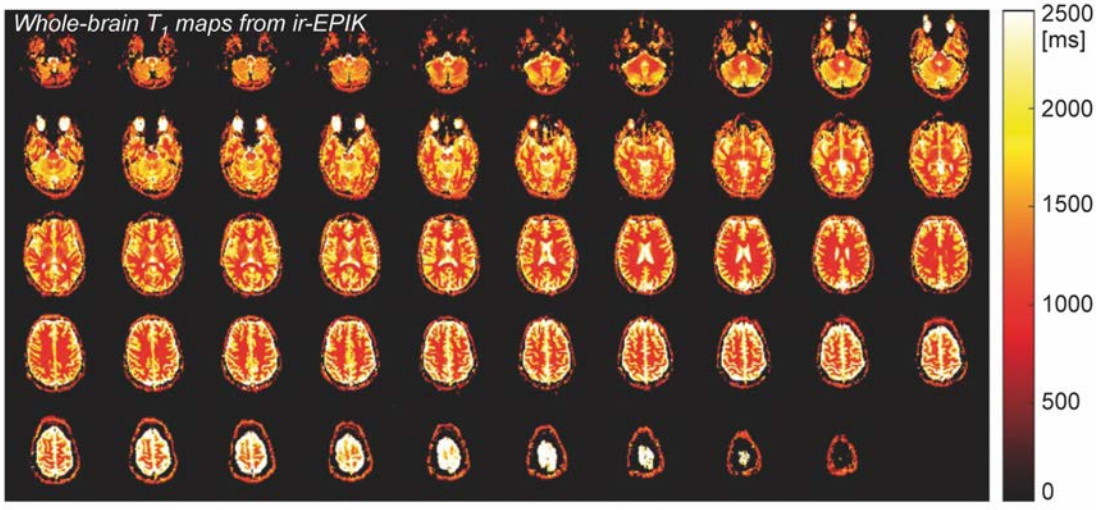

WHOLE-BRAIN HALF-MILLIMETRE FMRI RESTING-STATE NETWORKS AT 7T (I)

TR-external EPIK

Despite the advancements of fMRI acquisition techniques, the spatial resolution achieved in several recent works has remained around $0.7 \times 0.7 \times 0.7\ mm^3$, and most methods are only able to provide limited brain coverage. Therefore, a novel fMRI method is presented, providing a half-millimetre in-plane resolution with whole-brain coverage. The imaging method was developed based on the combination of 'TR-external EPI phase correction' with 'EPIK', both of which have been shown to be effective in improving the spatial resolution and brain coverage while maintaining comparable BOLD detection performance when compared to a standard EPI method [5,6,10,11]. The developed imaging method is termed 'TR-external EPIK' [12].

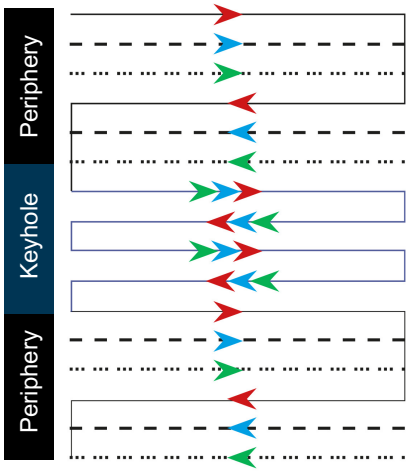

Key element1: EPIK

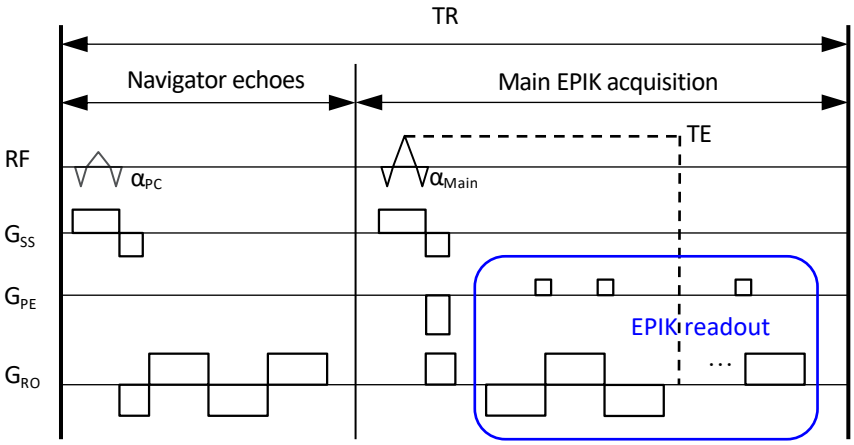

Key element2: TR-external EPI phase correction

Reconstructed images

The above TR-external EPIK scheme enabled a half-millimetre protocol with the imaging parameters shown in the table [12]. The above imaging configuration was employed on a Siemens Magnetom Terra 7T scanner with a single-channel Tx/32-channel Rx Nova medical coil supplied by the manufacturer. The figure below shows reconstructed images obtained from the half-millimetre protocol, taken from a single-volume functional scan at representative slice locations. The images are well reconstructed without any severe degradations and a detailed spatial representation of anatomical structures can be observed. The complete extent of the brain covered by TR-external EPIK can be verified from the coronal and sagittal images. It is important to note that the cortical ribbon can even be seen clearly in these resliced images. Moreover, all slices were shown to be reconstructed without any significant inter-slice artefacts,

	Parameters
TR/TE	3500/22 ms
FOV	210 x 210 mm^2
Matrix	408 x 408 (0.51 x 0.51 mm^2)
No. of slices	108 (axial; 1 mm)
Accele-ration	iPAT/multi-band/pF = 3/3/62.5%%

Imaging Parameters

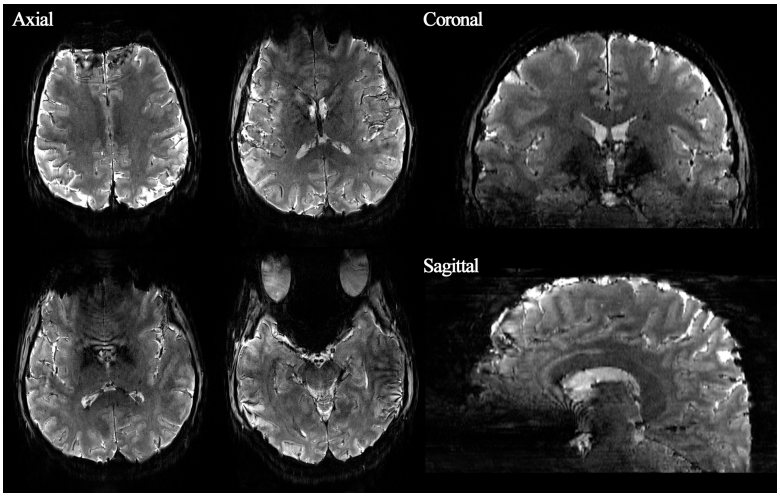

WHOLE-BRAIN HALF-MILLIMETRE FMRI
RESTING-STATE NETWORKS AT 7T (II)

Layer structures

From the axial slices, specific brain regions were chosen (marked by white rectangles: r_1–r_4) in which the following mesoscale anatomical structures can be observed (see Figure below): small cerebral vessels (red arrows in r_2) or the internal granular layer of the cortex (yellow arrows) located on the anterior wall of the postcentral gyrus (r_1), on the Heschl gyrus (r_3) or within the calcarine sulcus (r_4).

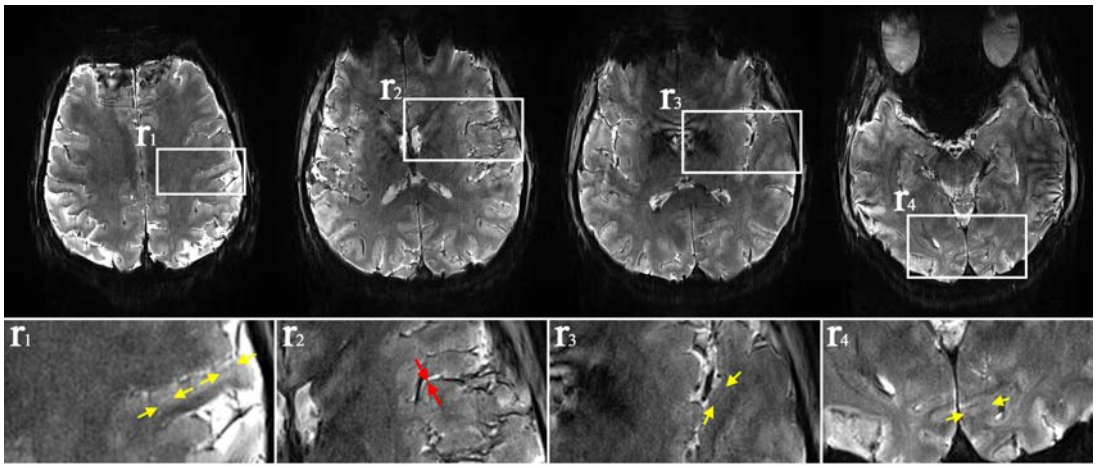

Resting-state networks

Figure below shows identified resting-state networks from TR-external EPIK: default mode, sensorimotor (LH), sensorimotor (RH), fronto-parietal (executive) and the visual network. This figure demonstrates that the extensive brain coverage provided by TR-external EPIK enabled the five RSNs to be simultaneously determined from a single fMRI session. In addition, the half-millimetre protocol (0.26 mm^3 voxels) enabled the identification of functional voxels very locally along the cortical ribbon.

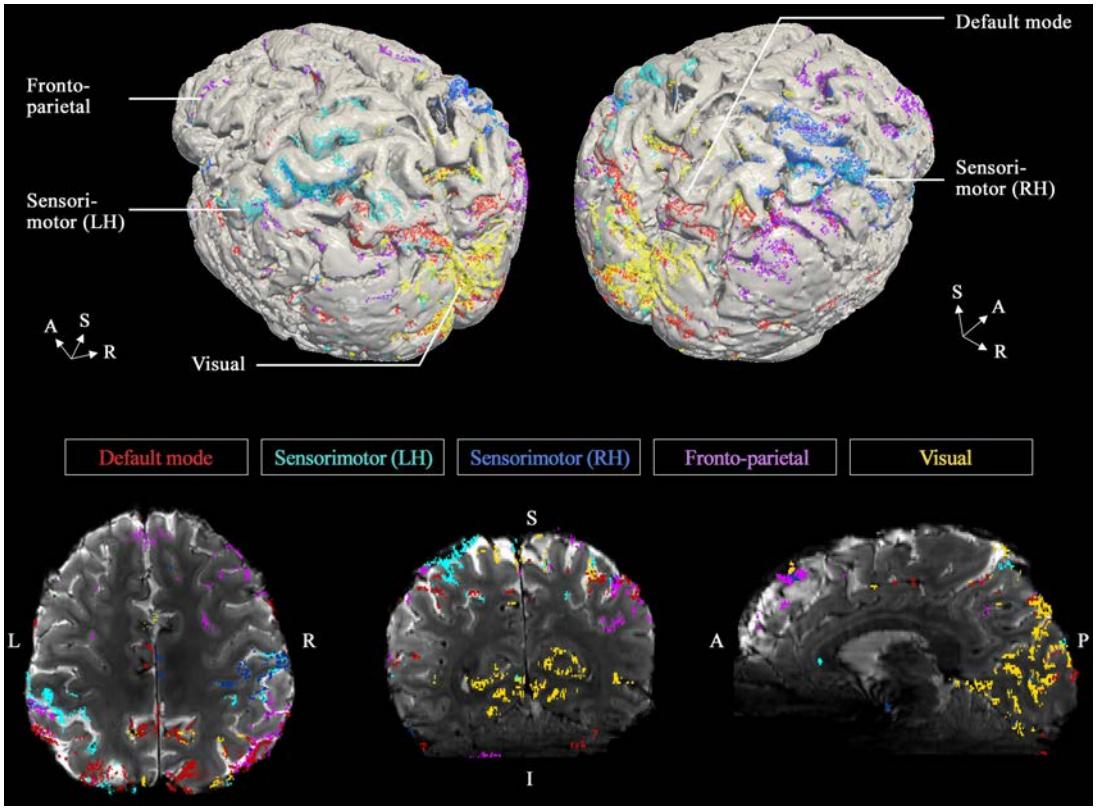

WHOLE-BRAIN HALF-MILLIMETRE FMRI
RESTING-STATE NETWORKS AT 7T (III)

Cortical depth dependent functional profiles

For each resting-state network (default mode, sensorimotor (RH) and visual), an ROI was selected (marked with a green rectangle) and is displayed in a magnified view. Here, twenty solid lines, starting from 'P_1' and ending at 'P_2' crossing the cortical ribbon, were manually defined and the network-specific probability profiles along the lines were examined. The results show signal variation within the cortical regions and the functional activation from the three networks is mostly confined to the GM regions.

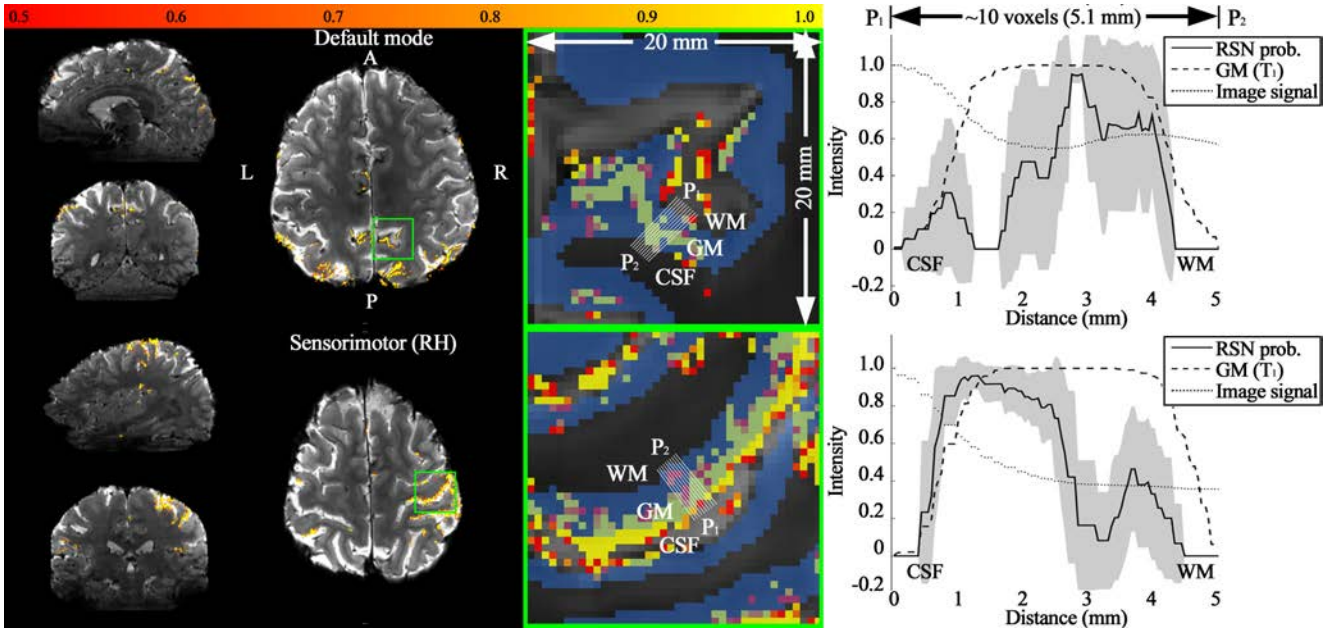

Imaging performance

Figure below shows the imaging parameters employed in our work (TR-external EPIK) in comparison to those in previous submillimetre-resolution fMRI studies. It has the highest in-plane spatial resolution (0.51 mm) compared to prior publications. Importantly, the spatial resolution was achieved with a sufficiently large in-plane FOV (210 mm), which can cover an entire normal, adult-sized brain sliced in any orientation, which is not the case in most prior studies. As a result, TR-external EPIK gives the largest number of voxels per temporal volume (17.98 M).

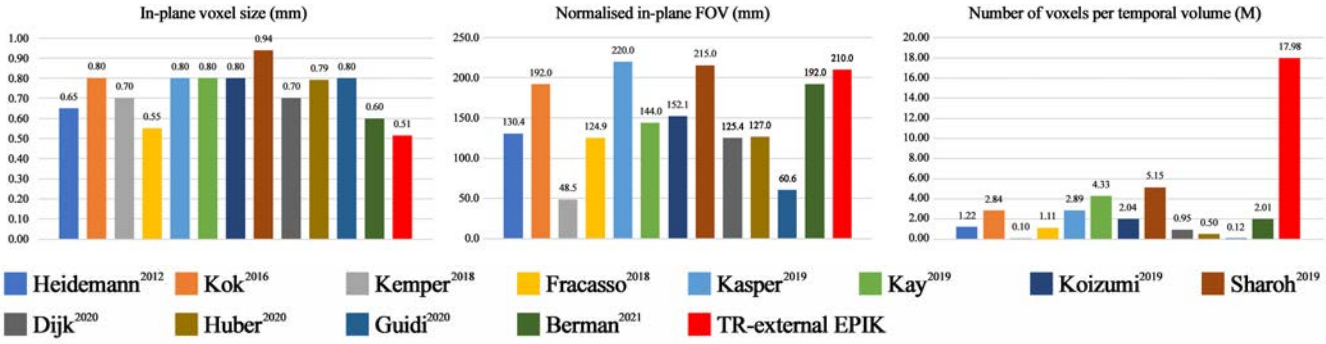

SUB-MILLIMETRE EPIK
EVOKED FMRI (I)

Depth-dependent evoked responses

Given that the cortical thickness is approximately 3 mm (see map on the right), **the sub-millimetre resolution achie-ved with EPIK allows the blood-oxygen-level-dependent (Bold) fMRI signal to be tracked across different corti-cal depths.** An MP2RAGE scan can be used to identify the outer ("pial") and inner ("white") boundaries of the cortical mantel, between which a number of intermediate surfaces can be generated. The EPIK fMRI scan (0.63 mm isovoxel) can then be projected to each of these surfaces to perform cortical-depth-dependent functional analysis.

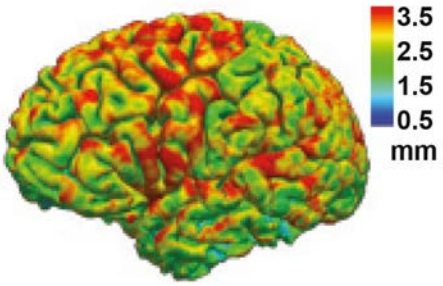

	PARAMETERS
TR/TE	3500/22 ms
FOV	210 x 210 mm^2
Matrix (Res.)	336 x 336 x 123 (0.63 mm^3)

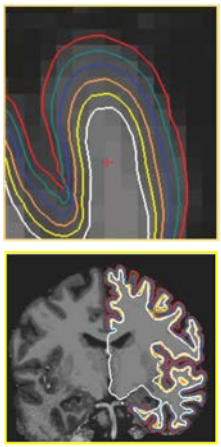

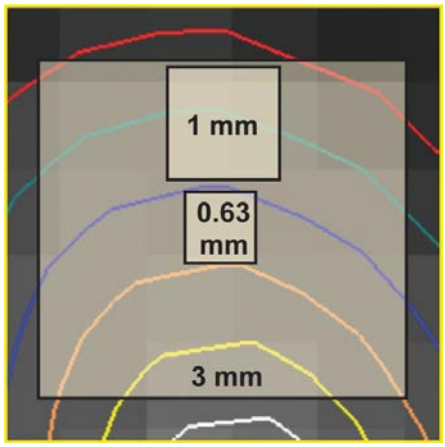

Correlates of finger tapping at 7T

Once the 4D-EPIK image is mapped onto MP2RAGE-based cortical surfaces, the general linear model (GLM) can be applied to the fMRI time course of each vertex. The images below show surface-based results of a motor task (bilateral finger tapping) at 0.63 mm isotropic resolution from a representative subject. The ROI-based results from four different volunteers are shown on the next page.

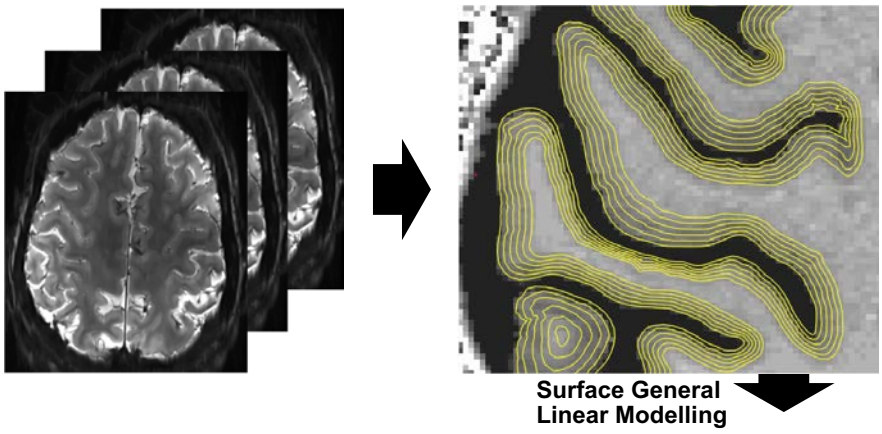

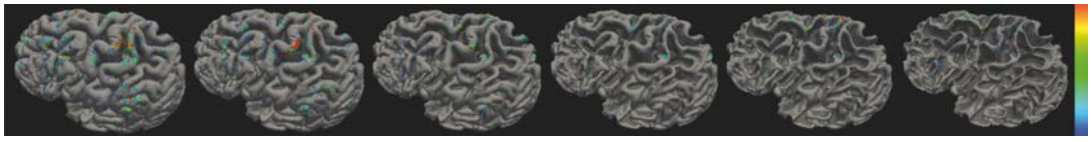

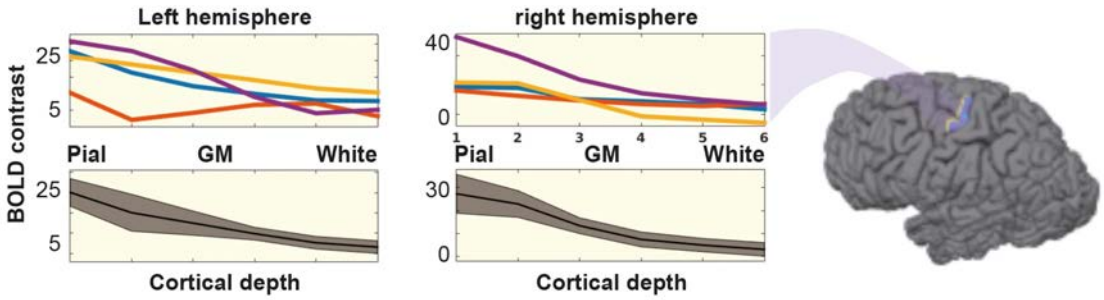

SUB-MILLIMETRE EPIK
EVOKED fMRI (II)

Line activation profiles

Besides a surface-based GLM, a routine volume-based GLM analysis can benefit from sub-millimetre resolution to identify **depth-dependent activations locally across a particular section of the cortex.** In the example below, a line-profile approach was used to demonstrate depth-dependent activations within a single axial slice. A group of 20 lines with a start point at the CSF and an end point in the white matter (WM) was manually defined to study depth-dependent activations of grey matter (GM) in the motor cortex. The intensity profile of all lines crossing the pre-central gyrus was generated for three different images: **(a)** a mean EPIK, **(b)** a cortical ribbon mask (obtained from a co-registered MP2RAGE) and **(c)** a statistic activation map computed in volume-space from a routine GLM. For each modality, the profiles of the 20 lines were averaged and plotted as mean intensity ± std (dashed lines) (see **d-f**). The average activation profile across the lateral portion of the omega-shaped pre-central gyrus was identified as the activation profile overlapping with the cortical ribbon (the part of the curve within the grey rectangle in Fig. **f**).

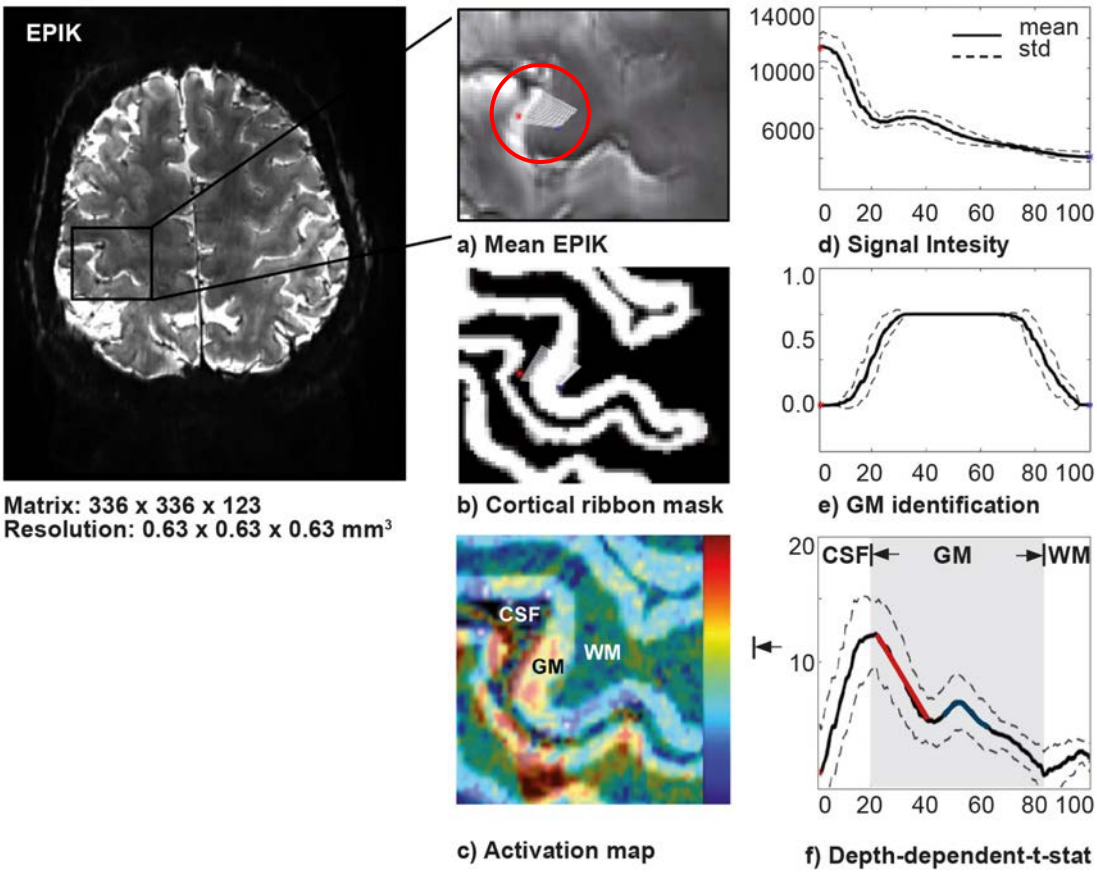

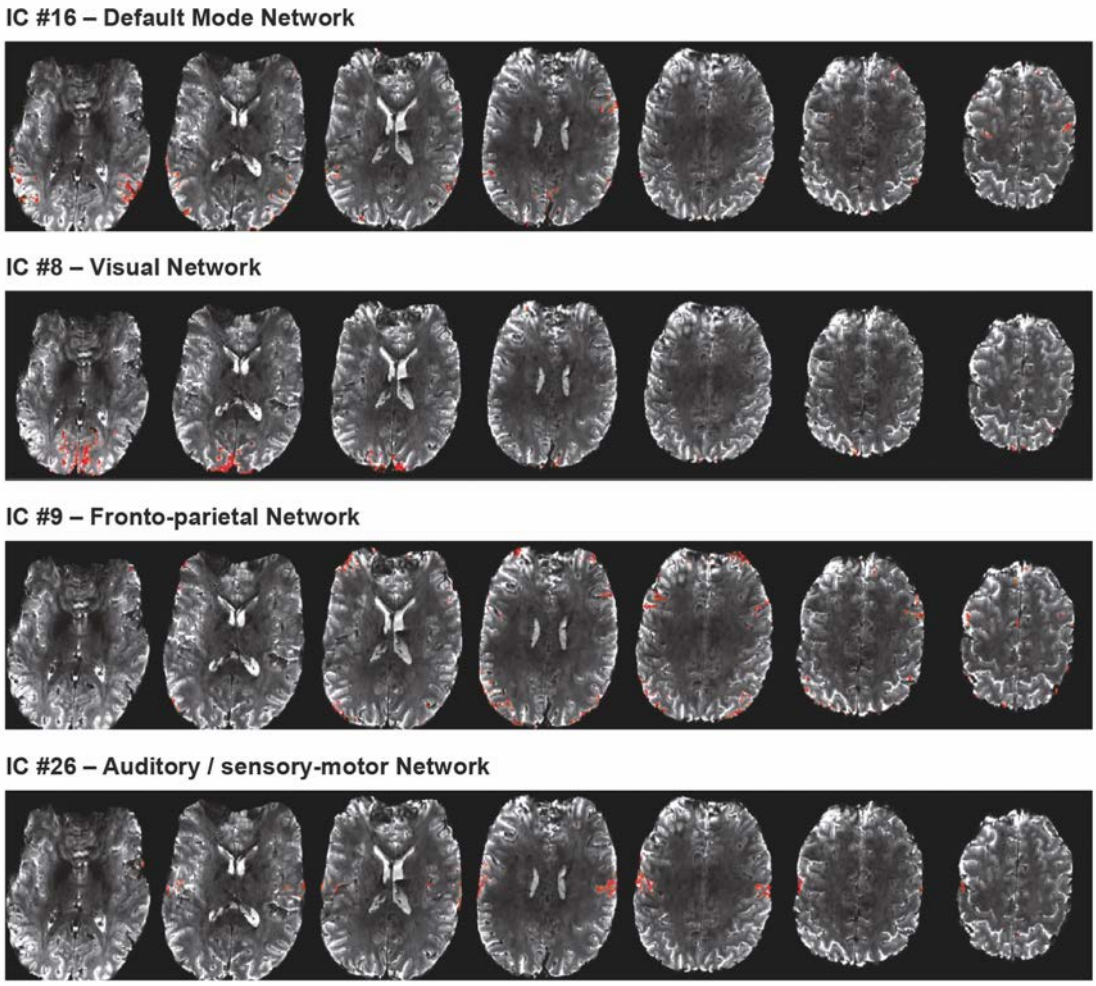

SUB-MILLIMETRE EPIK
rs-fMRI (I)

Cortical depth-dependent rs-fMRI oscillations

The high resolution and large coverage provided by EPIK make it possible to assess cross-regional connectivity including different cortical depths. As an initial step in the analysis of this multidi-mensional data (i.e., cortical areas and depths), the brain can be decomposed into functionally-different cortical regions using the co-registered MP2RAGE and an atlas-based automatic segmentation tool.

Once EPIK is mapped onto the cortical ROIs, several sub-ROIs can be generated as intermediate surfaces between the outer and the inner cortical boundaries. The time course of the vertices belonging to a particular sub-ROI can be averaged, resulting in ROI-depth functional units. The image below shows the average time course of an ROI at 6 cortical depths (BOLD amplitude encoded in greyscale).

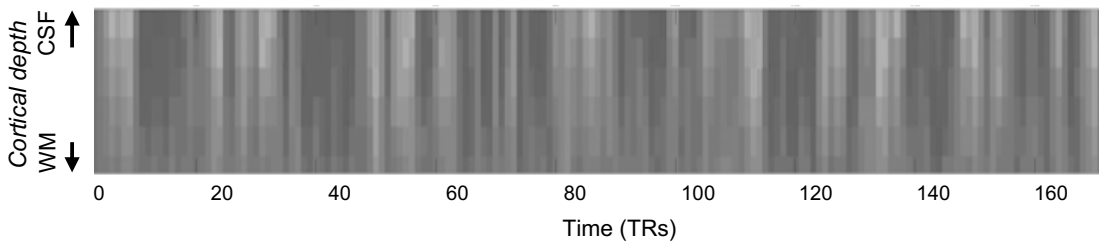

ROIs generated by Freesurfer from an 0.6 mm isotropic resolution MP2RAGE.

Functional time courses can be characterised based on their frequency content (power-frequency decomposition). Resting-state oscillations are believed to occur within a frequency range of 0.01 Hz - 0.1Hz, with slower frequencies typically associated with noise (and therefore, filtered during pre-processing). The spectral characteristics of the cortical signals can be analysed at different depths using EPIK (see graphs below). On the vertical axis of the spectral matrices, 28 ROIs are shown, each of them decomposed into six depths (for each ROI, the top row corresponds to the deepest layer – closest to white matter, and the bottom row to the more superficial layer – closer to the pial veins or the CSF). Superficial layers tend to show a higher power for nearly all frequencies.

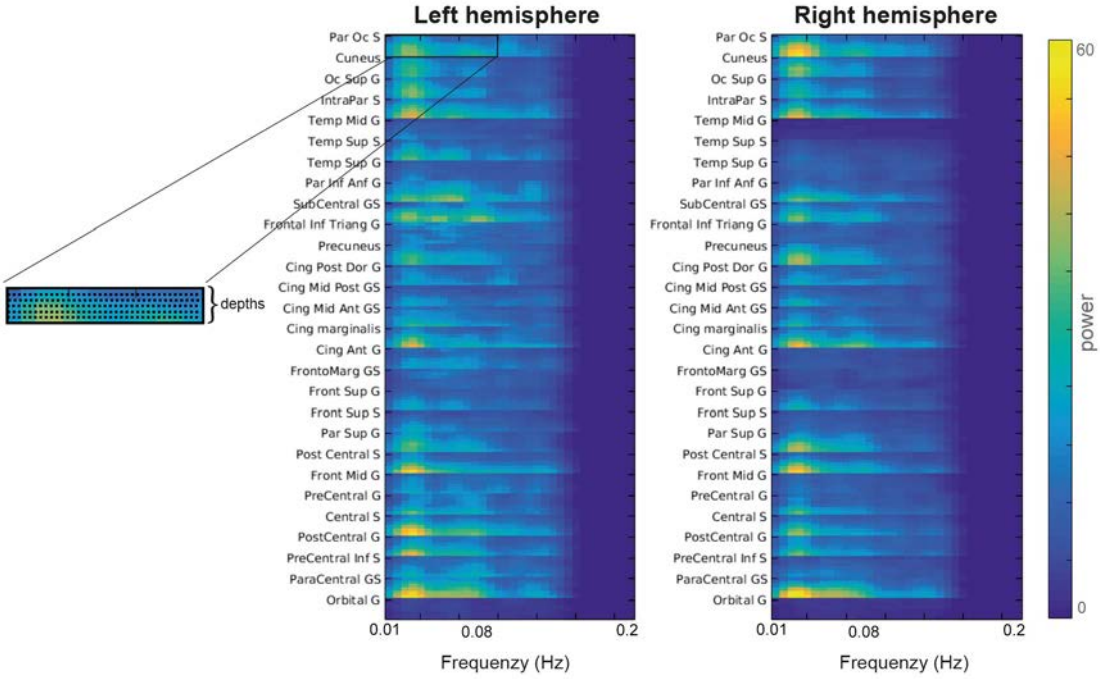

SUB-MILLIMETRE EPIK
rs-fMRI (II)

Cortical depth-dependent connections

The EPIK time course at each cortical layer from all ROIs can be correlated with every other compartmentalised time course in the cerebral cortex. **This renders a depth-dependent ROI connectivity matrix (on the next page).** Each marked division in this matrix contains the cross-ROI correlation values considering one seed ROI. The smaller sub-divisions (see magnified inset) correspond to six different cortical depths within each ROI.

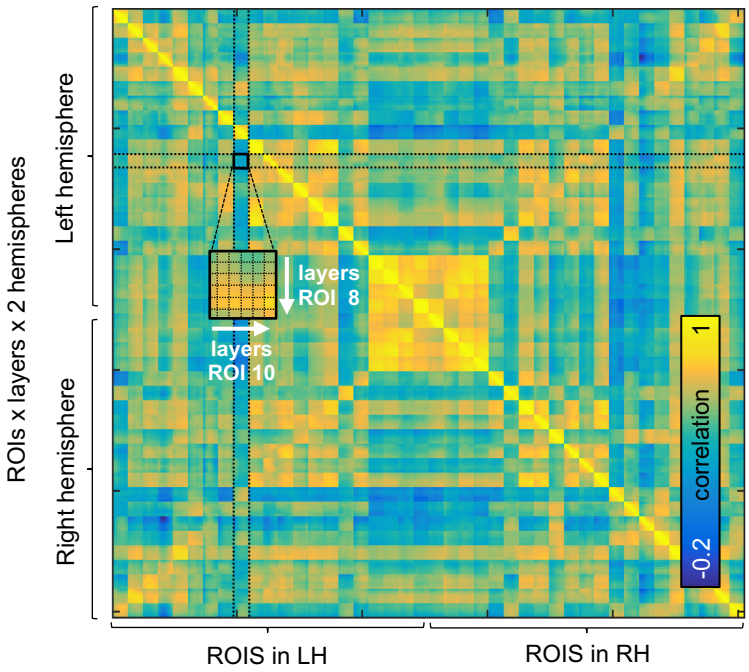

This high order connectivity matrix can be simplified as a connectivity graph by thresholding the correlation values. Furthermore, the ROIs of particular networks can be selected to report depth-dependent network connectivity. As an example, the two graphs below show the connections between ROIs of the default mode network (left) and the executive control network (right) that survive a correlation threshold of 0.4 and exhibited a p-value below 0.05 in a group t-test. Connections between different depths are colour-coded (see legend). Note the symmetry between both hemispheres, which suggests reliability of the connectivity results obtained from EPIK. Different line colours indicate connections at different cortical depths. The results of a cortical depth-specific network analysis in the healthy human brain are explained in detail in reference 16.

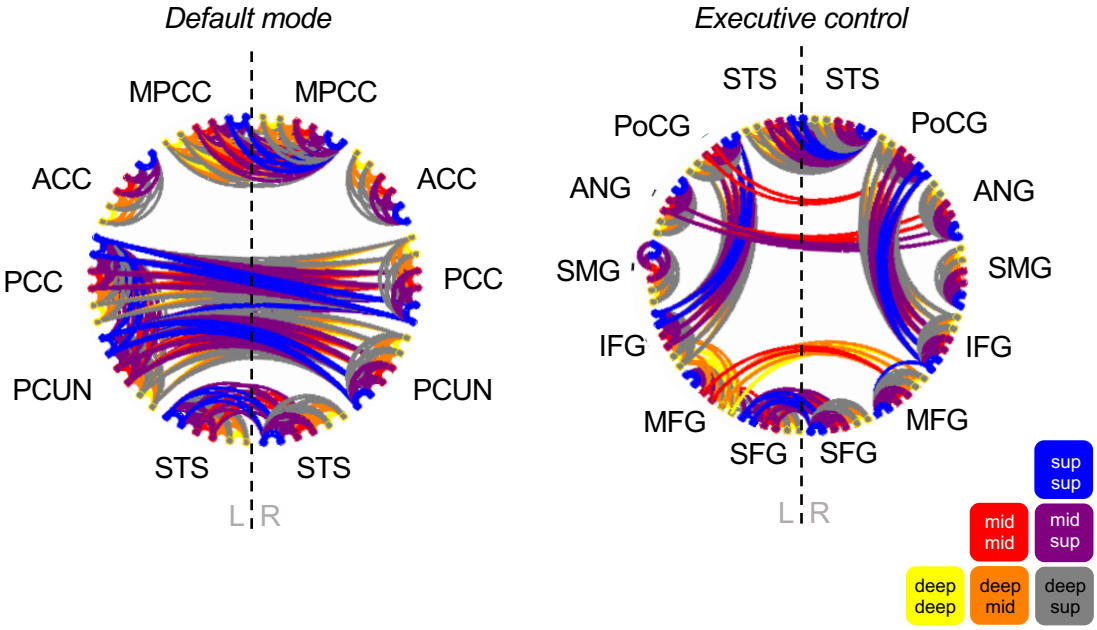

Impact of EPIK on rs-fMRI

Overall, rs-fMRI benefits greatly from EPIK because it enables scanning with high spatial resolution without compromising brain coverage. With these features, the function of the cerebral cortex in the human brain can be investigated in unprecedented detail, adding one dimension (cortical depth) to the investigation of cortical networks.

REFERENCES

PATENTS

1. Shah NJ, Zilles K. Verfahren zur Untersuchung eines Objektes mittels Erfassung des Ortsfrequenzraumes. German Patent 2003; Patent No. 199 62 845 C2.
2. Shah NJ, Zilles K. Imaging process in the spatial frequency space and useful for examining the properties of object. USA Patent 2004; Patent No. 6781372 B2.
3. Shah NJ, Zaitsev M., Leach M. O., Collins J. C., D'Arcy J. Keyhole Echo-Planar imaging with double (T_1 and T_2^*) Contrast (DC-EPIC); US Patent 2007; Patent No. 7 235 972 B2
4. Shah NJ, Zaitsev M., D'Arcy J., Collins D.J., Osmond M. Verfahren zur zeitabhängigen Wirkungsbestimmung eines Kontrastmittels. German Patent 2012; Patent No 102 2 1 795 B4.

JOURNALS

5. Zaitsev M, Zilles K, Shah NJ. Shared k-space echo planar imaging with keyhole. Magn Reson Med 2001;45:109-117.
6. Zaitsev M, Arcy JD, Collins DJ, Leach MO, Zilles K, Shah NJ. Dual-contrast echo planar imaging with keyhole: application to dynamic contrast-enhanced perfusion studies. Phys Med Biol 2005;50:4491-4505.
7. Yun S, Reske M, Vahedipour K, Warbrick T, Shah NJ. Parallel imaging acceleration of EPIK for reduced image distortions in fMRI. NeuroImage 2013;73:135-43.
8. Yun S, Shah NJ. Whole-brain high in-plane resolution fMRI using accelerated EPIK for enhanced characterisation of functional areas at 3T. PLoS One. 2017;12(9):e0184759.
9. Caldeira L, Kops E, Yun S, da Silva N, Mauler J, Weirich C, Scheins J, Herzog H, Tellmann L, Lohmann P, Langen K, Lerche C, Shah NJ. The Jülich Experience with Simultaneous 3T MRBrainPET: Methods and Technology. IEEE tran on radiation and plasma medical sciences. 2019;3:352-362.
10. Caldeira L*, Yun S*, da Silva N, Filss C, Shah NJ. Dynamic Susceptibility Contrast Parametric Imaging Using Accelerated Dual-Contrast Echo Planar Imaging With Keyhole. J Magn Reson Imaging. 2019;8:1-13.
11. Shah NJ, da Silva N, Yun S. Perfusion weighted imaging using combined gradient/spin echo EPIK: Brain tumour applications in hybrid MR-PET. Hum Brain Mapp. 2019;13:1-11.
12. Yun S*, Weidner R*, Weiss PH, Shah NJ. Evaluating the Utility of EPIK in a Finger Tapping fMRI Experiment using BOLD Detection and Effective Connectivity. Scientific Reports. 2019;10978.
13. Yun S, NJ Shah. Analysis of EPI Phase Correction with Low Flip Angle Excitation to reduce the required minimum TE: Application to Whole-Brain, Submillimetre-Resolution fMRI at 3T. Magn Reson Med. 2020 Sep;84(3):1416-1429.
14. Yun S, NJ Shah. Analysis of EPI Phase Correction with Low Flip Angle Excitation to reduce the required minimum TE: Application to Whole-Brain, Submillimetre-Resolution fMRI at 3T. Magn Reson Med. 2020 Sep;84(3):1416-1429.
15. Yun S, Pais-Roldán P, Palomero-Gallagher N, Shah NJ. Mapping of whole-cerebrum resting-state networks using ultra-high resolution acquisition protocols. Hum Brain Mapp. 2022 Aug 1;43(11):3386-3403. doi: 10.1002/hbm.25855. **(Cover-artwork for HBM August 1, 2022, Issue 43-11)**.
16. Pais-Roldán P, Yun S, Shah NJ. Pre-processing of sub-millimetre GE-BOLD fMRI data for laminar applications. Frontiers in Neuroimaging. 2022 doi: 10.3389/fnimg.2022.869454.
17. Küppers F, Yun S, Shah NJ. Development of a novel 10-echo multi-contrast sequence based on EPIK to deliver simultaneous quantification of T_2 and T_2* with application to oxygen extraction fraction. Magn Reson Med. 2022 Oct;88(4):1608-1623. doi: 10.1002/mrm.29305.

ABSTRACTS

18. Pais-Roldán P, Yun SD, Palomero-Gallagher N, Shah NJ. Cortical depth-dependent human fMRI of resting-state networks using EPIK. Frontiers in Neuroscience. 2023;17:1151544. doi: 10.3389/fnins.2023.1151544.
19. Yun S, Küppers F, Shah NJ. Submillimetre fMRI acquisition techniques for detection of laminar and columnar level brain activation. J Magn Reson Imaging 2023. doi: 10.1002/jmri.28911.
20. Yun S, Reske M, Vahedipour K, Warbrich T, Shah NJ. Reduced image distortions in fMRI using accelerated EPIK sequence at 3T. In: Proceedings of the 20th Annual Meeting of ISMRM, 2012.
21. Zhang K, Yun S, Neuner I, Filss C, Langen K-J, Shah NJ. Comparison of EPIK and Parallel EPI in Dual-Shot DSC. In: Proceedings of the 20th Annual Meeting of ISMRM, 2012.
22. Yun S, Shah NJ. Combination of Multiplexed EPI with EPIK (EPI with Keyhole) for Reduced Image Distortions at 3T. In: Proceedings of the 21st Annual Meeting of ISMRM, 2013.
23. Yun S, Shah NJ. Multiplexed EPI at 9.4T with PSF-based distortion correction. In: Proceedings of the 21st Annual Meeting of ISMRM, 2013.
24. Yun S, Shah NJ. Accelerated multiplexed-EPI with PSF-based distortion correction at 9.4T. In: Proceedings of the 22nd Annual Meeting of ISMRM, 2014.
25. Caldeira L, Yun S, da Silva NA, Filss C, Shah NJ. Estimation of the Arterial Input Function Using Accelerated Dual-Contrast EPIK: A Multi-Modality MR-PET Study. In: Proceedings of the 22nd Annual Meeting of ISMRM, 2014.
26. Yun S, Shah NJ. High-resolution fMRI using Accelerated EPIK for Enhanced Characterisation of Functional Areas at 3T. In: Proceedings of the 23rd Annual Meeting of ISMRM, 2015.
27. Caldeira L, Yun S, da Silva NA, Filss C, Shah NJ. Conversion of the arterial input function using accelerated dual-contrast EPIK: a multi-modality MR-PET study. In: Proceedings of the 23rd Annual Meeting of ISMRM, 2015.
28. Yun S, Shah NJ. Accelerated Multi-band EPIK for High-Resolution Dynamic MRI at 3T. In: Proceedings of the simultaneous multi-slice imaging (ISMRM workshop), 2015.
29. Yun S, Shah NJ. Full-FOV, whole-brain, half-millimetre in-plane readout-segmented EPIK for high-resolution fMRI studies. In: Proceedings of the 25th Annual Meeting of ISMRM, 2017; Abstract 1485.
30. Shah NJ, Yun S. A rapid, whole-brain look-locker method for T_1 mapping using inversion recovery EPIK. In: Proceedings of the 25th Annual Meeting of ISMRM, 2017;Abstract 3719.
31. Yun S, Shah NJ. On the Analysis of EPI Phase Correction with Small Tip Angle Excitation to reduce minimum required TE: Application to Whole-Brain Submillimetre-Resolution fMRI at 3T. In: Proceedings of the 26th Annual Meeting of ISMRM, 2018;Abstract 4245.
32. Yun S, Shah NJ. A fast and whole-brain quantitative mapping of T_1 using inversion recovery EPIK: method evaluation with TAPIR. In: Proceedings of the 6th International Congress on Magnetic Resonance Imaging (ICMRI), 2018;Abstract 2018_FA-043.
33. NJ Shah, Yun S. Rapid, whole-brain T_1 mapping using inversion recovery EPIK (ir-EPIK): a quantitative assessment with a group of subjects. In: Proceedings of the 27th Annual Meeting of ISMRM, 2019;Abstract 4970.
34. Yun S, NJ Shah. Full-FOV, Whole-brain, Half-millimetre Resolution fMRI at 7T using Accelerated multi-band EPIK with TR-external Phase Correction. Half mm, whole brain, full FOV fMRI. In: Proceedings of the 27th Annual Meeting of ISMRM, 2019; Abstract 1167. **(Oral presentation)**.
35. Yun S, Pais-Roldán P, Shah NJ. Detection of Cortical Depth-dependent Functional Activation using Whole-brain, Half-millimetre Resolution EPIK at 7T. In: Proceedings of the 28th Annual Meeting of ISMRM, 2020;Abstract 3863.
36. Pais-Roldán P, Yun S, Shah NJ. Cross-cortical Depth-dependent Interactions in the Human B rain using EPIK. In: Proceedings of the 28th Annual Meeting of ISMRM, 2020;Abstract 1366.
37. Küppers F, Yun S, Shah NJ. A Novel 10-echo GESE multi-parametric sequence based on the EPIK readout for simultaneous quantification of T_2 and T_2^*. In: Proceedings of the 28th Annual Meeting of ISMRM, 2020;Abstract 3863.

ABSTRACTS

38. Yun S, Pais-Roldán P, Palomero-Gallagher P, Shah NJ. Mapping of Whole-brain Resting-State Networks with Half-Millimetre Resolution using TR-external EPIK at 7T. In: Proceedings of the 29th Annual Meeting of ISMRM, 2021;Abstract 3376.
39. Pais-Roldán P, Yun S, Shah NJ. Pre-processing of high-resolution gradient-echo images for laminar fMRI applications. In: Proceedings of the 29th Annual Meeting of ISMRM, 2021;Abstract 2867.
40. Küppers F, Yun S, Shah NJ. Simultaneous quantification of T_2 and T_2^* by accelerated 10-echo GESE-EPIK sequence for carrageenan-phantoms and in vivo data. In: Proceedings of the 29th Annual Meeting of ISMRM, 2021;Abstract 1627.
41. Pais-Roldán P, Yun S, Shah NJ. High dynamicity of cortical depth-dependent connectivity states. In: Proceedings of the 30th Annual Meeting of ISMRM, 2022; Abstract 3903.
42. Küppers F, Yun S, Shah NJ. Rapid T_2' quantification by 10-echo GESE-EPIK sequence with application to oxygen extraction fraction imaging. In: Proceedings of the 30th Annual Meeting of ISMRM, 2022;Abstract 3944.
43. Oh S, Chang M, Kwak S, Choi J, Shah NJ, Yun S. Where is each finger area in brain? Enhanced characterization of the somatosensory area using high-resolution EPIK at 3T. In: Proceedings of the 31st Annual Meeting of ISMRM, 2023;Abstract 2720.
44. Küppers F, Yun S, Lohmann P, Filss C, Stoffels G, Langen K-J, Shah NJ. Rapid T_2' quantification by 10-echo GESE-EPIK sequence with application to oxygen extraction fraction imaging. In: Proceedings of the 31st Annual Meeting of ISMRM, 2023;Abstract 0764. **(Oral presentation)**.

SOFTWARE PACKAGE (C2P, SIEMENS)

45. Yun S. EPIK (EPI with Keyhole) for Magnetom Terra 7T VE12U SP01.Siemens Healthineers Teamplay (https://webclient.eu.api.teamplay.siemens-healthineers.com/c2p).18.Jul.2022.
46. Küppers F. GE-SE EPIK for MAGNETOM PRISMA VE11C-SP01 and VE11E. Siemens Healthineers Teamplay (https://webclient.eu.api.teamplay.siemens-healthineers.com/c2p). 18.Jul.2022.

BOOK CHAPTERS

47. Worthoff WA, Yun S, NJ Shah. Introduction to Magnetic Resonance Imaging. In: NJ Shah, editor. Hybrid MR-PET Imaging: Systems, Methods and Applications. Royal Society of Chemistry; 2018. p 1-44.
48. Yun S, Farrher E, Grinberg F, Oros-Peusquens AM, NJ Shah. Selective applications of MRI for the brain. In: NJ Shah, editor. Hybrid MR-PET Imaging: Systems, Methods and Applications. Royal Society of Chemistry; 2018. p 64-100.

* Indicates joint first authorship

CONTACT DETAILS

Prof. N. Jon Shah
Institute of Neuroscience and Medicine - 4
Forschungszentrum Jülich GmbH, 52425 Jülich
Germany, Email: n.j.shah@fz-juelich.de

Dr. Seong Dae Yun
Institute of Neuroscience and Medicine - 4
Forschungszentrum Jülich GmbH, 52425 Jülich
Germany, Email: s.yun@fz-juelich.de

Mitglied der Helmholtz-Gemeinschaft